IEEE Access
Multidisciplinary : Rapid Review : Open Access Journal

Received August 2, 2018, accepted August 30, 2018, date of publication September 17, 2018, date of current version October 8, 2018.

Digital Object Identifier 10.1109/ACCESS.2018.2869040

Enhanced Multi-Objective Teaching-Learning-Based Optimization for Machining of Delrin

ELANGO NATARAJAN[1], VARADARAJU KAVIARASAN[2], WEI HONG LIM[1], SEW SUN TIANG[1], AND TENG HWANG TAN[1]

[1]Faculty of Engineering, Technology and Built Environment, UCSI University, Kuala Lumpur 56000, Malaysia
[2]Department of Mechanical Engineering, Sona College of Technology, Salem 636005, India

Corresponding author: Elango Natarajan (cad.elango.n@gmail.com)

This work was supported by the Centre of Excellence for Research, Value Innovation and Entrepreneurship, UCSI University, through the Pioneer Scientist Incentive Fund under Project Proj-In-FETBE-034.

ABSTRACT This paper deals with the optimization of machining parameters of speed, feed rate, and depth of cut that aim to simultaneously achieve the low surface roughness (SR) and high material removal rate (MRR) of a version of ACETAL homopolymer material known as Delrin. First, an L27 orthogonal array with three-level of cutting speed (V_c), feed rate (f), and depth of cut (ap) is formulated, and the experiments are conducted accordingly in a CNC turning machine using cemented carbide tool with insert angle of 80°. A response surface model is rendered from these experimental results, and two objective functions representing the SR and MRR of Delrin are derived. An enhanced multi-objective teaching–learning-based optimization (EMOTLBO) is then proposed to solve the multi-objective machining problem, aiming to minimize the SR and maximize the MRR of Delrin simultaneously. A fuzzy decision maker is also integrated to softly select the preferred solution from Pareto-front based on the importance level of both objective functions. Extensive simulation studies prove that EMOTLBO is more competitive than other existing algorithms for being able to produce a more uniformly distributed Pareto-front. Simulation results are further validated Experimentally, and the difference of lower than 5% is observed that imply to good agreement between the simulation and experimental results.

INDEX TERMS Homopolymer, multi-response, design of experiment (DOE), response surface model (RSM), analysis of variance (ANOVA), surface roughness (SR), material removal rate (MRR), enhanced teaching-learning-based optimization (EMOTLBO).

I. INTRODUCTION

Delrin is an engineering crystalline thermoplastic polymer material developed by DuPont. It is a version of Acetal homopolymer that offers an excellent physical, tribological and environmental properties that make it suitable for many mechanical and industrial applications. It is generally difficult to machine due to its properties like low elastic modulus, rate of moisture absorption, high coefficient of thermal expansion, and internal stresses. It is a challenge to achieve both surface finish and material removal rate concurrently as these parameters represent quality and quantity respectively. While human process planner can utilize their experiences to determine the machining parameters, the selected values are generally conservative and largely deviated from optimum settings. Meanwhile, the determination of optimum process parameters through experiments are tedious and high cost.

Substantial researches were conducted to address these difficulties in the past. Various regression models were derived by the researchers based on experimental data to map the relationship between the input and output parameters, aiming to achieve better prediction of the performance of machining processes of the selected material. Chabbi *et al.* [1] investigated the influence of machining parameters, i.e., the cutting force and cutting power on material removal rate in turning of polyoxymethylene (POM C) using L27 orthogonal array. They used Response Surface Model (RSM) for modeling and artificial neural network for optimization and reported that feed rate is the most significant parameter for improving surface finish, while the feed rate and depth of cut are crucial for improving material removal rate. Kaddeche *et al.* [2] investigated the surface roughness, cutting force, and temperature rise during the machining of HDPE 80 and HDPE 100 polymers and reported that feed rate affects the surface roughness and depth of cut influences the temperature level. Also revealed that the temperature generated in the cutting zone of HDPE 80 is higher than that of HDPE 100. Panda *et al.* [3] studied the influence of machining parameters on surface roughness (SR) and material removal rate (MRR) in turning of Nylon 6/6 using analysis of variance (ANOVA). It was reported that SR decreases when both cutting speed and feed rate increase. Lazarevića *et al.* [4] used L27 Taguchi orthogonal array to study the influences of four cutting parameters; cutting speed, feed rate, depth of cut and tool nose radius to minimize the SR in turning of polyethylene. ANOVA was also performed to identify the importance level of these process parameters. Hamlaoui *et al.* [5] investigated the machinability of HDPE tough resin used for piping and fittings. Gaitonde *et al.* [6], [7] used Taguchi method and ANOVA to study better machinability during the turning of unreinforced polyamide (PA6) and glass fiber reinforced polyamide (PA66GF30). They reported that PCD tool is better than cemented carbide (K10) for machining PA6 and PA66GF30 and optimal values of feed rate and cutting speed should be kept at low level to achieve better results. The effect of cutting speed and feed rate on surface finish in the machining of Ultra High Molecular Weight Polyethylene (UHMWPE) was studied in [8], while the machinability of unreinforced polyetheretherketone (PEEK) and glass fiber reinforced (GF30) PEEK was studied in [9] using Taguchi method. The machinability study on carbon reinforced PEEK material was conducted in [10], while Abdul Shukor *et al.* [11] focused on applying Taguchi method to determine the best machining parameters for pocket milling process of polypropylene (PP). In [12], all factors that influence the SR of glass fiber reinforced resin were assessed using design of experiments (DOE) and ANOVA. In [13], the surface roughness in turning of polyamide was modeled and optimized using artificial neural network by considering the feed rate, cutting speed, depth of cut and tool nose radius as control parameters.

Most of the regression models seen in literatures are nonlinear functions consist of several input machining parameters with bounded values. One approach used to determine the optimum parameter settings is to integrate these regression model with optimization methods. Although the conventional optimization algorithms such as geometric programming, nonlinear programming, dynamic programming etc. can be employed to solve the regression models, these approaches need an excellent guess of initial solution for not being trapped into the local optima [14]. Due to their robustness in searching process, various evolutionary algorithms and swarm intelligence algorithms were recently designed and integrated into the regression models to achieve optimum solutions. A comprehensive study of works that utilizing evolutionary algorithms and swarm intelligence algorithms to address optimization of machining parameters can be found in [15]–[17].

Most machining problems are formulated and solved using multi-objective optimization because machining is involved with more than one performance characteristic simultaneously. Two popular methods known as the priori approach and the posterior approach [18] are commonly used to solve these multi-objective optimization problems (MOPs). Unlike the priori approach that can only generate a unique optimum solution in a single run based on a specific combination of weight, the posterior approach can generate a set of multiple tradeoff or Pareto-optimal solutions of a MOP using a single simulation run. Posterior approach also allows the process planner to decide a unique optimum solution from the Pareto-optimal solutions based on the importance level of each objective without requiring them to know these importance levels in advance [19]. For these reasons, the posterior approach is preferred over the priori approach in solving the MOPs of machining process that need to consider the frequent change of customer requirements.

Various types of multi-objective evolutionary algorithms (MOEAs) were reported to solve MOPs. The frameworks of MOEAs can be categorized into two types, namely Pareto-dominance-based (e.g., ε-MOEA, SPEA2 and PESA) [20]–[22] and decomposition-based (e.g., MOEA/D and NSGA-III) [23], [24]. The existing MOEAs adopted one of these approaches to obtain the non-dominated solution set. In [25], an imperialist competitive algorithm was used to tackle the multi-response optimization of ultrasonic machining process. In [26], particle swarm optimization (PSO) was used to multi-objective optimization of electric discharge machining. A multi-objective Jaya algorithms was recently proposed in [27] to solve the four modern machining processes known as the wire-electric discharge machining (WEDM) process, laser cutting process, electro-chemical machining (ECM) process and focused ion beam (FIB) micro-milling process.

Recently, teaching-learning-based optimization (TLBO) [28] and its variants have been widely used to solve different machining parameter optimization problems due to the advantage of not requiring any algorithm-specific control parameters. A multi-objective TLBO (MOTLBO) was used in [29] to minimize both of the carbon emission and operation time of turning operations simultaneously. A non-dominated sorting TLBO was proposed in [30] to solve four machining processes of WEDM, laser cutting, ECM and FIB micro-milling. More variants of MOTLBO and their applications can be found in [31]–[38]. For instance, a multi-objective improved teaching-learning based optimization (MO-ITLBO) was reported in [34] to solve the MOPs with the results of statistical analyses by integrating ε-domination method into ITLBO. An identical MO-ITLBO was also reported in [35]. In [36], MO-ITLBO was applied to optimize the design of a plate-fin heat exchanger. While the MO-ITLBO variants reported in [34]–[36] seems to be same, none of these works can clarify how an ITLBO can be extended to solve the MOPs [37]. A multi-objective individualized-instruction teaching-learning based optimization were designed in [38] to solve MOPs more effectively by designating specific teacher to improve learner's knowledge and adopting the external archive to preserve promising solutions found.

The objective of this paper is to investigate the multi-objective machining parameters optimization of Delrin. Despite of its high requirement for industrial application, the machining characteristics of Delrin have not been addressed so far based on the authors' best knowledge. In this paper, the research contributions are presented with two major areas. The first area (in Section II) focuses on design of experiments (DOE), the regression model developed based on the experimental results and two objective functions representing minimizing surface roughness and maximizing material removal rate of the selected material. The second area (in Section III) focuses on a posterior version of MOEA known as the enhanced multi-objective teaching-learning-based optimization (EMOTLBO) to obtain the optimum turning conditions of Delrin in order to simultaneously minimize surface roughness and maximize material removal rate. Some modifications and improvements are also proposed in EMOTLBO to solve MOPs effectively. An external archive is integrated into EMOTLBO to store or retrieve the non-dominated Pareto optimal solutions. Different selection mechanisms for teacher and peer learner are introduced to facilitate better guiding effect during the teacher and learner phases of EMOTLBO. A mutation operator is designed to prevent the stagnation on local Pareto front by emulating a brainstorming session that promotes the critical thinking of learner. An archive controller is designed to insert the newly obtained non-dominated solutions and eliminate the redundant archive members. Finally, a fuzzy decision maker [39] is also integrated in EMOTLBO to softly select the most preferred compromised solution from the set of Pareto optimal solution based on the order of importance of objectives.

The simulation and experimental results are presented in Section IV, while the conclusions are presented in Section V.

TABLE 1. Properties of Delrin (from the supplier).

Property	Value
Density	1411.67514 kg/m^3
Specific gravity	1420 kg/m^3
Tensile strength @ yield 73° F	62.05282 MPa
Compressive strength	35.85274 MPa
Flexural strength	79.289709 MPa
Melting point	347° F
Elongation @ break, 73° F	25%
Dynamic coefficient of friction (40 psi, 50 fpm)	0.2

II. EXPERIMENTAL MODELING OF DELRIN

A. EXPERIMENTAL DETAILS

A cylindrical Delrin rod of 30 mm diameter was chosen as the material, while CNC turning center model sprint 16TC (Fanuc 0i T Mate C) CNC with Fanuc control motors and drives was chosen for the machining. Table 1 presents the mechanical and physical properties of Delrin, while

TABLE 2. Cutting tool specification (from the tool manual).

Description	Code	Specification
Grade	CNMG	CNMG 120408 QM
Insert Shape and angle	C	Rhombic 80°
Insert clearance angle	N	0°
Tolerance	M	±0.13
Insert size	iC	12.0 mm
Insert thickness	S	4.76 mm
Nose radius	r_ε	0.8 mm
Suitability	QM	Suitable for mixed production
Tool Material	HC	Cemented Carbide

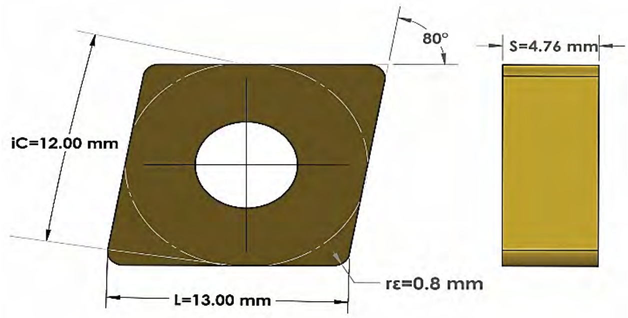

FIGURE 1. Cutting tool geometry.

TABLE 3. Machining parameters and their levels.

Machining Parameters	Level I	Level II	Level III
Cutting speed, V_c (*m/minute*)	90	135	180
Feed rate, f (*mm/rev*)	0.1	0.3	0.5
Depth of cut, ap (*mm*)	0.5	1.0	1.5

Table 2 shows the specification of the carbide tip (CNMG) cutting tool insert. Figure 1 shows the geometry of the cutting tool. Servo super cut coolant32 was used for turning three steps of equal length of 10 mm. Three levels of cutting speed V_c (*m/minute*), feed rate f (*mm/rev*) and depth of cut ap(*mm*) as recommended by cutting tool manufacturer was considered and L27 matrix was built as shown in Table 3. Figure 2 shows the machined specimen and chips during machining.

(a) (b)

FIGURE 2. (a) Machined specimen and (b) chips during the machining.

Surface finish denoted as R_a (μm) and material removal rate denoted as MRR(cm^3/*minute*) were considered as response variables. Surface roughness of each sample was instantly measured using Mitutoyo make surf tester after

TABLE 4. Experimental results of Ra and MRR with control variables.

Run Number	Machining Variables			Response Variables	
	V_c (m/minute)	f (mm/rev)	ap (mm)	R_a (μm)	MRR (cm^3/minute)
1	90	0.1	0.5	0.79	4.50
2	90	0.1	1.0	0.61	9.00
3	90	0.1	1.5	0.56	13.50
4	90	0.3	0.5	1.88	13.50
5	90	0.3	1.0	1.78	27.00
6	90	0.3	1.5	1.74	40.50
7	90	0.5	0.5	1.67	22.50
8	90	0.5	1.0	1.59	45.00
9	90	0.5	1.5	1.65	101.25
10	135	0.1	0.5	1.18	6.750
11	135	0.1	1.5	0.84	20.25
12	135	0.1	1.0	0.66	13.50
13	135	0.3	0.5	1.60	20.25
14	135	0.3	1.5	1.72	60.75
15	135	0.3	1.0	1.66	40.50
16	135	0.5	0.5	1.50	33.75
17	135	0.5	1.5	1.80	101.25
18	135	0.5	1.0	1.43	67.50
19	180	0.1	0.5	1.19	9.00
20	180	0.1	1.5	0.89	27.00
21	180	0.1	1.0	0.67	18.00
22	180	0.3	0.5	1.62	27.0
23	180	0.3	1.5	1.65	81.00
24	180	0.3	1.0	1.60	54.00
25	180	0.5	0.5	1.42	45.00
26	180	0.5	1.5	1.61	135.00
27	180	0.5	1.0	1.59	90.00

each machining. Each measurement was done four times and the mean of measurement of these four trials was recorded as in Table 4. The *MRR* was calculated empirically based on the rate at which volume of material removed as:

$$MRR = V_c \times f \times ap \tag{1}$$

B. RESPONSE SURFACE METHODOLOGY

Response Surface Methodology (RSM) is an experimental modeling technique used to determine relationship between control variables and response variables. The objective of using RSM in this research is to investigate the effect of cutting speed (V_c). feed rate (f) and depth cut (ap) on surface finish R_a and material removal rate *MRR*.

In general, a second order RSM model is given by

$$Y = \alpha_0 + \sum_{i=1}^{I} \beta_i x_i + \sum_{i=j}^{I} \beta_{ij} x_i x_j + \sum_{i=1}^{I} \beta_{ii} x_i^2 \tag{2}$$

where α_0 is a free term of the regression equation; x_1, $x_2, \ldots, x_n$ are variable terms; β_i are linear coefficient terms, β_{ii} are quadratic coefficients; and β_{ij} are interacting coefficient terms. Let $\psi_1(\cdot,\cdot,\cdot)$ and $\psi_1(\cdot,\cdot,\cdot)$ be the functions to relate the response variables R_a and *MRR*, respectively, with the three control variables of V_c, f and ap where

$$R_a = \psi_1(V_c, f, ap) \tag{3}$$

$$MRR = \psi_2(V_c, f, ap) \tag{4}$$

The regression models of (3) and (4) are the second order full quadratic regression. The coefficients of α_0, β_i, β_{ii} and β_{ij} are determined based on the experimental data. The regression equations of R_a and *MRR* were obtained as:

$$\begin{aligned} R_a = {} & 0.86381 + 0.006238V_c + 7.44875f - 1.9865ap \\ & - 0.0016666 \times V_c \times f + 0.001888 \times V_c \times ap \\ & + 1.6 \times f \times ap - 0.0000312V_c^2 - 11.39375f^2 \\ & + 0.607ap^2 \end{aligned} \tag{5}$$

$$\begin{aligned} MRR = {} & 23.3431 - 0.1277V_c - 115.5125f - 30.095ap \\ & - V_c \times f + 0.3 \times V_c \times ap + 135.15 \times f \times ap \\ & - 0.00063827V_c^2 - 32.6875f^2 - 5.23ap^2 \end{aligned} \tag{6}$$

C. ANALYSIS OF VARIANCE

Analysis of variance (ANOVA) is a statistical tool used to determine how well a model fits the experimental data and examine the goodness-of-fit. The key parameters of the output of ANOVA are represented as S, P and R^2. Parameter S represents the standard deviation of how far the data values fall from the fitted values and indicates how well the model describes the response. R^2 is the percentage of variation of data in the response with the range of 0-100%. Higher value of R^2 indicates the better fit of model. The significance is generally checked as: (i) if the value of probability $P < 5\%$, the model is adequate and parameters are significant on responses and (ii) if the value of $P > 5\%$, the model is adequate and parameters are insignificant on responses. The experimental data shown in Table 4 and the developed RSM model were input into a statistical tool in which a confidence level of 95% was set in order to find the model adequacy. The percentage of contribution of each machining parameter on response variable was calculated.

D. PROBLEM FORMULATION OF DELRIN MACHINING

The multi-objective machining optimization of Delrin can be formulated based on the regression models obtained from (5) and (6). Three process parameters considered in the multi-objective machining model of Delrin are cutting speed (V_c), feed rate (f) and depth cut (ap). Surface roughness (R_a) and material removal rate (*MRR*) that respectively represent the quality and quantity of product, are two contradictory objectives to be optimized simultaneously.

To this end, the multi-objective machining optimization problem of Delrin material can be expressed as:

$$\begin{aligned} & \begin{cases} \underset{V_c,f,ap}{\text{minimize}}\ R_a \\ \underset{V_c,f,ap}{\text{maximize}}\ MRR \end{cases} \\ \text{s.t. } & 80m/minute \le V_c \le 200m/minute \\ & 0.09mm/rev \le f \le 0.5mm/rev \\ & 0.5mm \le ap \le 3.0mm \end{aligned} \tag{7}$$

The optimum machining parameters of V_c, f and ap for multi objective optimization problem of (7) are solved using the proposed EMOTLBO. For the ease of implementation, the maximization of MRR can be equivalently represented as the minimization of negative value of MRR.

III. PROPOSED METHODOLOGY

A. TLBO

TLBO was proposed in [28] to emulate the interaction between teacher and learners during the learning process in a classroom. The best solution of each generation represents teacher, while the remaining candidate solutions are learners. The learners are able to accept instructions from teacher and learn from other peers as well.

Let $X_{n,d}^{g}$ be the d-th dimension of the n-th learner in g-th generation for $n \in [1, N]$, $d \in [1, D]$ and $g \in [1, G]$, where N is the population size; D is the total number of design variable; and G is the total generation. Denote $\bar{X}_{d}^{g}$ and $X_{T,d}^{g}$ as the d-th dimension of mean and best (teacher) solutions, respectively. The d-th dimension of each n-th learner $X_{n,d}^{g}$ can be updated in teacher phase as follow:

$$X_{n,d}^{g+1} = X_{n,d}^{g} + r_1 \left(X_{T,d}^{g} - T_f \bar{X}_{d}^{g} \right) \tag{8}$$

$$\bar{X}_{d}^{g} = \frac{1}{N} \sum_{n=1}^{N} X_{n,d}^{g} \tag{9}$$

where r_1 is a random number between 0 to 1 generated from uniform distribution; T_f is the teaching factor and it can be set as either 1 or 2 with equal probability to reflect the teaching ability of X_{T}^{g}. The new solution X_{n}^{g+1} produced in teacher phase can replace the current solution X_{n}^{g} if the former solution has better fitness than the latter one.

The completion of teacher phase leads to learner phase that emulates peer-learning mechanism among the learners. Each updated learner X_{n}^{g+1} can interact with a randomly selected peer X_{r}^{g+1} to improve its knowledge further, where $r \in [1, N]$ and $r \neq n$. The learner X_{n}^{g+1} is attracted by its peer X_{r}^{g+1}, if the latter solution has better fitness than the former one and vice versa. Denote $\tilde{X}_{n,d}^{g+1}$ as the d-th dimension of n-th learner produced during the learner phase, then:

$$\tilde{X}_{n,d}^{g+1} = X_{n,d}^{g+1} + r_2 \left(X_{r,d}^{g+1} - X_{n,d}^{g+1} \right), \quad \text{if } X_{r}^{g+1} \text{ is fitter than } X_{n}^{g+1} \tag{10}$$

$$\tilde{X}_{n,d}^{g+1} = X_{n,d}^{g+1} + r_2 \left(X_{n,d}^{g+1} - X_{r,d}^{g+1} \right), \quad \text{if } X_{n}^{g+1} \text{ is fitter than } X_{r}^{g+1} \tag{11}$$

where r_2 is a random number between 0 to 1 generated from uniform distribution. The new solution $\tilde{X}_{n}^{g+1}$ obtained from learner phase can replace the current solution X_{n}^{g+1} if the former solution is fitter than the latter one.

The TLBO algorithm begins optimization by generating a set of N random solutions as the first population. During optimization, each learner gradually moves closer to teacher or peers with better fitness and repels away from peers with worse fitness using (8)-(11) to achieve good balance of intensification and diversification of search process. The position vector of teacher is returned as the best solution of optimization when the termination conditions are met.

Since the inception of TLBO, it has been applied to solve various engineering problems as reported in [28] and [40]–[42]. Apart from exploring the potential applications of TLBO, some studies focused on analyzing the implementation of TLBO and its convergence characteristic. Črepinšek *et al.* [43] attempted to replicate the experimental results of Rao *et al.* [40], [41] and some notable findings in terms of performance comparisons between algorithms. A geometric interpretation of TLBO was used in [44] to explore its inherent origin bias, the impacts on the population convergence and success rates of objective functions with origin solutions.

B. EMOTLBO

1) EXTERNAL ARCHIVE

In the beginning of EMOTLBO, an initial population is randomly generated with N learners denoted as X_{n}^{g}. Assume that M is the total number of objective functions considered, the m-th objective function value of learner X_{n}^{g} is evaluated as $F_m \left(X_{n}^{g} \right)$, where $m = 1, \ldots, M$. Unlike the single objective optimization that allows easy comparison between solutions using relational operator, solutions of multi-objective space needs to be compared using the Pareto dominance concept due to trade-off between different objectives [45]. A solution is better than (dominates) another solution if and only if the former one shows better or equal objective value on all of the objectives and provide a better value in at least one of the objective functions. All non-dominated solutions found in the initialization stage is stored in a fixed-size external archive that consists of a space with dimensions equal to the number of objective functions considered. The objective space in archive is divided into multiple equally-spaced hypercubes to maintain the uniform distribution of non-dominated solutions and prevent the loss of good solutions.

2) TEACHER AND PEER SELECTION MECHANISM

All learners in the proposed EMOTLBO are updated using the teacher phase and the learner phase represented by (8)-(9) and (10)-(11), respectively. The best solution obtained so far in EMOTLBO is used as the teacher to guide other learners towards the promising regions of search space in order to find a near global optimum solution. Nevertheless, it is challenging to find the best solution of multi-objective search space due to various trade-offs between objectives. Different selection mechanisms are designed for teacher and learner phases of EMOTLBO to address this issue.

For teacher phase, a teacher is selected from the existing Pareto optimal solutions stored in external archive. Since all archive members are non-dominated with each other, the density of each occupied hypercube in archive becomes main consideration during the selection mechanism of teacher phase. The less occupied hypercube tends to be chosen to offer one of its non-dominated solutions as teacher. Let c be a constant number greater than one, K_h be number of Pareto optimal solutions exist in the h-th occupied hypercube and H be total number of occupied hypercube in external archive. Define P_h as the probability of each h-th occupied hypercube

Algorithm 1: X_T^g **= Select_Teacher(** A^g **)**

Calculate the total number of occupied hypercube H based on the current archive A^g;
*/*for each h-th occupied hypercube */*
for $h = 1$ to H **do**
    Calculate the number of Pareto optimal solution K_h exist in the h-th occupied hypercube;
    Calculate the selection probability of the h-th occupied hypercube P_h to offer teacher using (12);
end for
Use roulette-wheel method to select the h-th occupied hypercube to offer teacher based on P_h;
if selected hypercube has more than 1 **then**
    Randomly select one archive member from h-th occupied hypercube as teacher X_T^g;
end if

FIGURE 3. The pseudo-code for the selection of teacher.

to be chosen to offer teacher. The selection mechanism of teacher phase can be achieved using roulette-wheel method by referring to the probability P_h of each occupied hypercube defined as:

$$P_h = \frac{c}{K_h} \tag{12}$$

As shown in (12), the probability of choosing an occupied hypercube to offer teacher increases with decreasing number of non-dominated solutions in hypercube. A non-dominated solution in the chosen hypercube is randomly selected as teacher to update all EMOTLBO learners during the teacher phase using (8)-(9). Figure 3 shows the pseudo-code for the selection of teacher in each g-th generation based on the current external archive A^g. The updated learner X_n^{g+1} produced in teacher phase can replace the current learner X_n^g if the former solution dominates the latter one. Otherwise, X_n^{g+1} is discarded. If both X_n^{g+1} and X_n^g solutions are non-dominated with each other, a coin is flipped to determine which solution to be accepted. The pseudo-code used for the updating the solution of each n-th learner in the g-th generation is described in Figure 4.

Algorithm 2: X_n^{g+1} **= Update_Learner(** X_n^{new} **,** X_n^g **)**

Check the Pareto dominance relationship between new solution X_n^{new} and current solution X_n^g;
if X_n^{new} dominates X_n^g **then**
    $X_n^{g+1} \leftarrow X_n^{new}$;
else if X_n^g dominates X_n^{new} **then**
    $X_n^{g+1} \leftarrow X_n^g$;
else // both solutions are non-dominated to each other
    Randomly generate a number *rand* between 0 to 1;
    if *rand* < 0.5 **then**
        $X_n^{g+1} \leftarrow X_n^{new}$;
    else
        $X_n^{g+1} \leftarrow X_n^g$;
    end if
end if

FIGURE 4. The pseudo-code for updating the new solution of learner.

For learner phase, a peer learner X_k^{g+1} is randomly selected form population to update the learner X_n^{g+1} using (10) or (11).

Algorithm 3: X_k^{g+1} **= Select_Peer(** Pop^g **,** n**)**

/Pop^g refers to current population, n is the index of learner to be updated, k is the index of randomly selected peer, where n ≠ k.*/*
while n is equal to k **do**
    Randomly generate index $k \in [1, N]$;
    Compare the indices k and n;
end while
Return X_k^{g+1} as the peer of n-th learner;

FIGURE 5. The pseudo-code for the selection of peer learner.

Figure 5 shows the pseudo-code for the selection of peer for in each n-th learner during the peer-learning phase. The learner X_n^{g+1} is attracted towards its peer X_k^{g+1} as stated in (10) if the latter solution dominates the former one. Otherwise, the learner is repelled away from its peer using (11) to prevent learning from inferior peer learner. If both X_n^{g+1} and X_k^{g+1} solutions are non-dominated with each other, a coin is flipped to randomly select one equation from (10) and (11) to update X_n^{g+1} in learner phase. The same procedures as explained in teacher phase are then used to determine the updated n-th learner by considering the Pareto dominance levels between the solutions $\tilde{X}_n^{g+1}$ and X_n^{g+1}.

3) BRAINSTORMING SESSION

Although the density of each occupied hypercube in archive is designated as an auxiliary evaluation indicator to select teacher, the algorithm might be trapped into local optima due to the changes of population tends towards stability when the iterative generation becomes larger. This drawback leads to frequent selection of the least occupied hypercube to offer teacher. The guiding effect of randomly selected peer learner is also questionable when no significant change is observed in population diversity. This is challenging for the algorithm to escape from the local optimal especially when a given problem has complex Pareto front.

A probabilistic-based mutation operator is incorporated into EMTLBO to provide perturbation on the learners with probability of P_{mut} after they are updated from the teacher and learner phases. The mutation operator is analogous to the brainstorming session in a classroom that encourages the learners to think out of box after interacting with teacher and peers. Assume that the n-th learner plans to do brainstorming after updating the knowledge either from teacher or learner phases, the d-th dimension of n-th learner, i.e., $X_{d,n}^g$, is randomly chosen for perturbation as shown:

$$X_{d,n}^g = r_3 \left(X_d^U - X_d^L \right) \tag{13}$$

where r_3 is a random number between 0 to 1 generated from uniform distribution, while X_d^U and X_d^L are the upper and lower limits of d-th variable, respectively. The pseudo-code of brainstorming session is described in Figure 6. Similar procedures as explained in both teacher and learner phases are used to update the n-th learner by comparing the Pareto dominance levels between the current solution

Algorithm 4: X_n^{new} = **Brainstorming(** X_n^{new} , D, X^U, X^L**)**

Randomly generate a dimension index of $d \in [1, D]$;
Extract d-th component of X_n^g , X^U and X^L;
Perform perturbation on $X_{d,new}^g$ using (13);
Return X_{new}^g as the perturbed learner;

FIGURE 6. The pseudo-code for brainstorming session of learner.

Algorithm 5: A^{g+1} = **Archive_Controller(** A^g , Pop^{g+1}**)**

Assign new archive $A^{g+1} \leftarrow A^g$;
*/*for each updated learner in population Pop^{g+1}*/*
for $n = 1$ to N **do**
  / for each member in current archive A^{g+1}*/*
  for $a = 1$ to $|A|$ **do**
    Check the Pareto dominance relationship between X_n^{g+1} from Pop^{g+1} and $X_a^{Arc,g}$ from archive;
    if State == 1 **then** */* $X_a^{Arc,g}$ is dominated*/*
      Mark $X_a^{Arc,g}$ as dominated solution;
    else
      Break;
    end if
  end for
  Delete the marked dominated solutions from A^{g+1} ,
  if State != -1 **then** */* X_n^{g+1} is not dominated*/*
    Add X_n^{g+1} into A^{g+1} ;
    if X_n^{g+1} outside of outside the hypercube **then**
      Update the grids to cover X_n^{g+1} ;
    end if
    if Archive A^{g+1} is full **then**
      Calculate the crowding distance CD_a of each archive member in A^{g+1} using (14);
      Remove the most crowded archive member with lowest CD_a;
    end if
  end if
end for

FIGURE 7. The pseudo-code of the proposed archive controller.

and that obtained from the brainstorming session. For every n-th learner selected for brainstorming, no fitness evaluation is needed after obtaining new solution from the teacher or learner phases. Perturbation on these updated solutions is first performed using (13), followed by the fitness evaluation of perturbed solution.

4) ARCHIVE CONTROLLER

For each generation, a set of new solutions are produced in population via the teacher and learners phases, as well as the brainstorming session. The new non-dominated solutions in population are identified using the Pareto dominance concept and compared against the archive members in order to update the archive. Since the external archive is a fixed size storage unit, an archive controller is proposed to determine whether a new solution can be added into archive and which archive members need to be eliminated when the archive is full.

Figure 7 describes the pseudo-code of proposed archive controller. In general, the established rules used by archive controller to update the archive are summarized as follows:

- If the new member is dominated by at least one of the archive member, the archive controller prohibits the new member to enter archive.
- If the new member dominates at least one of the archive members, the archive controller deletes all dominated archive members and adds the new member into archive.
- If the new member and all archive members are non-dominated with each other, the archive controller adds the new member into archive.
- If the new member is inserted outside the hypercube in archive, the archive controller needs to rearrange the segmentation of objective spaces so that all hypercube in archive are extended to cover the new member.
- If the archive is full, the archive controller needs to eliminate the redundant archive members.

In contrast to the teacher selection mechanism explained earlier, crowding distance [46] is used by archive controller to estimate the density of solutions surrounding an archive member. The crowding distance CD_a of each a-th archive member $X_a^{Arc,g}$ is measured as the average distance of two adjacent members on either sides of the a-th archive member along each of the M objectives. Let $|A|$ be the total number of archive member A in current Pareto front and the crowding distance of each a-th archive member is initialized as $CD_a = 0$ for $a = 1, \ldots, A$. For every m-th objective function, all archive members are sorted in ascending order based on their objective value and stored in a list denoted as L_m. Assume that a-th archive member is sorted as the j-th element of list L_m, i.e., $L_m[j]$. The crowding distance of each j-th sorted member with objective value $F_m\left(X_{L_m[j]}^{Arc,g}\right)$ is:

$$CD_{L_m[j]} = \begin{cases} \infty, & \text{if } j = 1 \text{ or } j = A \\ CD_{L_m[j]} + \dfrac{F_m\left(X_{L_m[j+1]}^{Arc,g}\right) - F_m\left(X_{L_m[j-1]}^{Arc,g}\right)}{F_m\left(X_{L_m[F]}^{Arc,g}\right) - F_m\left(X_{L_m[1]}^{Arc,g}\right)}, & \\ & \text{if } j = 2, \ldots, (A-1) \end{cases} \quad (14)$$

From (14), the boundary solutions for each m-th objective function in the sorted list L_m have largest crowding distance. The archive members located on the less populous (isolated) regions of external archive have larger crowding distance and vice versa. When the archive is fully occupied, the proposed archive controller removes the archive members with lowest crowding distance in order to avoid the clustering of Pareto front on a single non-dominated solution. Unlike MOPSO and MOGWO where the extra archive member is randomly selected from the most occupied hypercube, EMOTLBO removes solution with the lowest crowding distance to ensure the less crowded member is not deleted accidentally.

5) FUZZY DECISION MAKER

One of the most challenging issues encountered by process planner is to select the most preferred solution of the multi-objective machining optimization problem by referring to the relative importance level of each objective function. A fuzzy decision maker [30] is incorporated into EMOTLBO to softly select the most preferred compromised solution among all Pareto optimal solutions based on the requirement or order of importance of objectives stated by customers.

Let $F^U = [F_1^U, \ldots, F_m^U, \ldots, F_M^U]$ be the utopia point defined as a specific point in the objective space where all objective functions are simultaneously at their best possible values. In contrary, pseudo nadir point is a point in the objective space where all objective functions are simultaneously at their worst value and denoted as $F^{SN} = [F_1^{SN}, \ldots, F_m^{SN}, \ldots, F_M^{SN}]$. To determine the most preferred solution from Pareto front, the fuzzy decision maker first calculates a linear membership function value for each m-th objective function in each Pareto optimal solution by measuring the relative distance between the value of the objective function in the Pareto optimal solution from its values in the respective utopia and pseudo nadir points. The closer value of objective function to its utopia point leads to higher membership function value that implies for higher degree of optimality for the objective function in the Pareto optimal solution and vice versa. Denote μ_a^m as the membership function value of each a-th archive member or Pareto optimal solution for the m-th objective function. For minimization problem, the value of μ_a^m is computed using the fuzzification process as shown:

$$\mu_a^m = \begin{cases} 1, & F_m\left(X_a^{Arc,G}\right) \leq F_m^U \\ \dfrac{F_m^{SN} - F_m\left(X_a^{Arc,G}\right)}{F_m^{SN} - F_m^U}, & F_m^U \leq F_m\left(X_a^{Arc,G}\right) \leq F_m^{SN} \\ 0, & F_m\left(X_a^{Arc,G}\right) \geq F_m^{SN} \end{cases} \tag{15}$$

For maximization problem, the value of μ_a^m is computed as:

$$\mu_a^m = \begin{cases} 0, & F_m\left(X_a^{Arc,G}\right) \leq F_m^{SN} \\ \dfrac{F_m\left(X_a^{Arc,G}\right) - F_m^{SN}}{F_m^U - F_m^{SN}}, & F_m^{SN} \leq F_m\left(X_a^{Arc,G}\right) \leq F_m^U \\ 0, & F_m\left(X_a^{Arc,G}\right) \geq F_m^U \end{cases} \tag{16}$$

Define w_m as the relative importance of the m-th objective function. The total membership function or total degree of optimality of each a-th Pareto optimal solution is computed by considering the individual membership function and the relative importance of each objective function as:

$$\mu_a = \sum_{m=1}^{M} w_n \mu_a^m \tag{17}$$

Based on (17), the a-th Pareto optimal solution with highest value of μ_a is selected as the most preferred non-dominated solution because this solution more optimizes the objective functions of multi-objective machining problem than other Pareto solutions based on the given relative importance. Figure 8 describes the pseudo-code of fuzzy decision maker.

Algorithm 6: $X_a^{Arc,desired}$ **= Fuzzy_Decision_Maker(** A^{Final} **,** M, w_m**)**

*/*Evaluate all M objectives for each archive member in final archive* A^{Final}**/*
for $a = 1$ to $|A|$ **do**
  for $m = 1$ to M **do**
    Evaluate the m-th objective function value of $X_a^{Arc,final}$;
  end for
end for
Generate utopia point $F^U = \left[F_1^U, \ldots, F_m^U, \ldots, F_M^U\right]$ based on the best values of all objective functions;
Generate pseudo nadir point $F^{SN} = \left[F_1^{SN}, \ldots, F_m^{SN}, \ldots, F_M^{SN}\right]$ based on the worst values of all objective functions;
for $a = 1$ to $|A|$ **do**
  for $m = 1$ to M **do**
    Calculate membership function value μ_a^m using (15) or (16);
  end for
  Calculate total membership function μ_a using (17);
end for
Find $X_a^{Arc,final}$ with the largest value of μ_a and then return it as the desired optimal solution of $X_a^{Arc,desired}$;

FIGURE 8. **The pseudo-code of fuzzy decision maker.**

6) THE COMPLETE EMOTLBO ALGORITHM

The pseudo-code of complete EMOTLBO is shown in Figure 9, where *fes* is the number of function evaluations and *max_fes* is the maximum function evaluations. During the initialization phase, a population of N learners is randomly generated, while the external archive A^g is initialized to be empty. After evaluating the objectives of each learner, the proposed archive controller is executed to keep the non-dominated solutions in archive. The teacher phase, learner phase, brainstorming session and external archive updating process of EMOTLBO are then executed cycle by cycle until the termination condition is met. At the termination of EMOTLBO, the Pareto optimal solutions stored in external archive are obtained. The desired Pareto optimal solution can be determined with fuzzy decision maker based on the predefined preference value of each objective function.

7) PERFORMANCE METRICS

Two performance metrics are used to evaluate the quality of Pareto optimal solution produced by all multi-objective algorithms in solving the Delrin machining optimization problem. Coverage to two sets [47] is a metric used to compare a pair of non-dominated solution sets by calculating the percentage of each set that is dominated by another set. Let $C(\cdot, \cdot)$ be the coverage operator, the coverage to two non- dominated solution sets of A and B are then defined as:

$$C(A, B) = \frac{|\{b \in B; \exists a \in A : a \prec= b\}|}{|B|} \tag{18}$$

The value $C(A, B) = 1$ implies that all solutions of set B are dominated or equal to all solutions in set A, while none of the solution in set B are covered by the set A is represented as $C(A, B) = 0$. The value of $C(A, B)$ is not necessary

Algorithm 7: EMOTLBO

$A^g = \{\}$; *//Empty archive*
$fes = 0$; *//Initialize fitness evaluation number*
for $n = 1$ to N **do**
    Randomly initialize the position of n-th learner;
    Evaluate all M objectives of n-th learner;
end for
$fes \leftarrow fes + N$;
A^g = **Archive_Controller(** A^g, Pop^{g+1}**);**
while $fes < max\_fes$ **do**
    for $g = 1$ to G **do**
        */*Teaching phase of EMOTLBO*/*
        Calculate population mean using (9);
        X_T^g = **Select_Teacher(** A^g **);**
        for $n = 1$ to N **do**
            Calculate new solution X_n^{new} using (8);
            */*Perform brainstorming with probability P_{mut}*/*
            Randomly generate $rand \in [0,1]$;
            if $rand \leq P_{mut}$ **then**
                X_n^{new} = **Brainstorming(** X_n^{new}, D, X^U, X^L**);**
            end if
            Evaluate all M objectives of new solution X_n^{new};
            X_n^{g+1} = **Update_Learner(** X_n^{new}, X_n^g **);**
        end for
        $fes \leftarrow fes + N$;
        */*Peer learning phase of EMOTLBO*/*
        for $n = 1$ to N **do**
            X_k^{g+1} = **Select_Peer(** Pop^g, n**);**
            if X_k^{g+1} dominates X_n^{g+1} **then**
                Calculate X_n^{new} using (10);
            else if X_n^{g+1} dominates X_k^{g+1} **then**
                Calculate X_n^{new} using (11);
            else */* X_n^{g+1} and X_k^{g+1} are non-dominated*/*
                Randomly generate $rand \in [0,1]$;
                if $rand < 0.5$ **then**
                    Calculate X_n^{new} using (10);
                else
                    Calculate X_n^{new} using (11);
                end if
                */*Perform brainstorming with probability P_{mut}*/*
                Randomly generate $rand \in [0,1]$;
                if $rand \leq P_{mut}$ **then**
                    X_n^{new} = **Brainstorming(** X_n^{new}, D, X^U, X^L**);**
                end if
                Evaluate all M objectives of new solution X_n^{new};
                X_n^{g+1} = **Update_Learner(** X_n^{new}, X_n^g **);**
            end if
        end for
        $fes \leftarrow fes + N$;
        A^{g+1} = **Archive_Controller(** A^g, Pop^{g+1}**)**
    end for
end while
$X_a^{Arc,desired}$ = **Fuzzy_Decision_Maker(** A^{Final}, M, w_m**);**

FIGURE 9. The pseudo-code of complete EMOTLBO.

equal to that of $1 - C(B, A)$, hence it is imperative to consider both of $C(A, B)$ and $C(B, A)$ during the performance comparison.

Spacing measure [48] is a metric used to quantify the uniformity distribution along the Pareto front obtained from different algorithms. Let the total objective functions and total non-dominated solutions in an archive be M and A, respectively. For every m-th objective, the smallest Euclidean distance between the a-th archive member and any b-th archive member in the objective space is computed as:

$$d_a = \min_{a,a\neq b} \sum_{m=1}^{M} \left| F_m\left(X_a^{Arc,G}\right) - F_m\left(X_b^{Arc,G}\right) \right|, \quad a, b = 1, \ldots, A \tag{19}$$

Meanwhile, the average of all d_a is obtained as:

$$\bar{d} = \frac{\sum_{a=1}^{A} d_a}{|A|} \tag{20}$$

Let S be the spacing measure and it is defined as the distance variance of neighboring non-dominated solutions, i.e.,

$$S = \sqrt{\frac{1}{|A-1|} \sum_{a=1}^{A} \left(\bar{d} - d_a\right)^2} \tag{21}$$

The value of $S = 0$ implies that all non-dominated solutions stored in external archive are equidistantly spaced from each other and it is the best possible performance.

IV. EXPERIMENTAL STUDIES

The first part of experimental studies focused on investigating how well the developed regression models of Delrin can fit into the experimental data. Extensive simulation and experimental studies were then conducted to evaluate the performance of EMOTLBO.

A. EVALUATION ON DELRIN MODELING

1) CONTOUR AND 3-D SURFACE PLOTS FROM RSM

The contour plots and 3D surface plots for R_a are presented in Figures 8(a)-(c) to provide better perceptive on the effect of input machining parameters V_c, f and ap on response variable R_a. Figures 9(a)-(c) show the contour plots and 3D surface plots for MRR, which were produced based on the experimental results reported in Table 4, in which one of the variable was set constant at its midst level and the remaining variables were interacted with each other.

Figure 10(a) shows the relations of V_c and f on R_a with fixed ap. The expected value of R_a is in the range of $0.6495 \leq R_a \leq 0.8596$ μm with lower f and higher V_c. If the f and V_c are increased further, R_a increases correspondingly. The effect of V_c and ap on R_a with constant f is illustrated in Figure 10(b). The expected value of R_a varies in the range of $1.5983 \leq R_a \leq 1.6009$ μm with higher V_c and higher ap. If V_c and ap are increased further, R_a increases accordingly. Figure 10(c) reveals the effect of f and ap on R_a when V_c is constant. The R_a value ranges as $0.6994 \leq R_a \leq 0.8019$ μm with lower f and higher ap. From these analyses, it can be

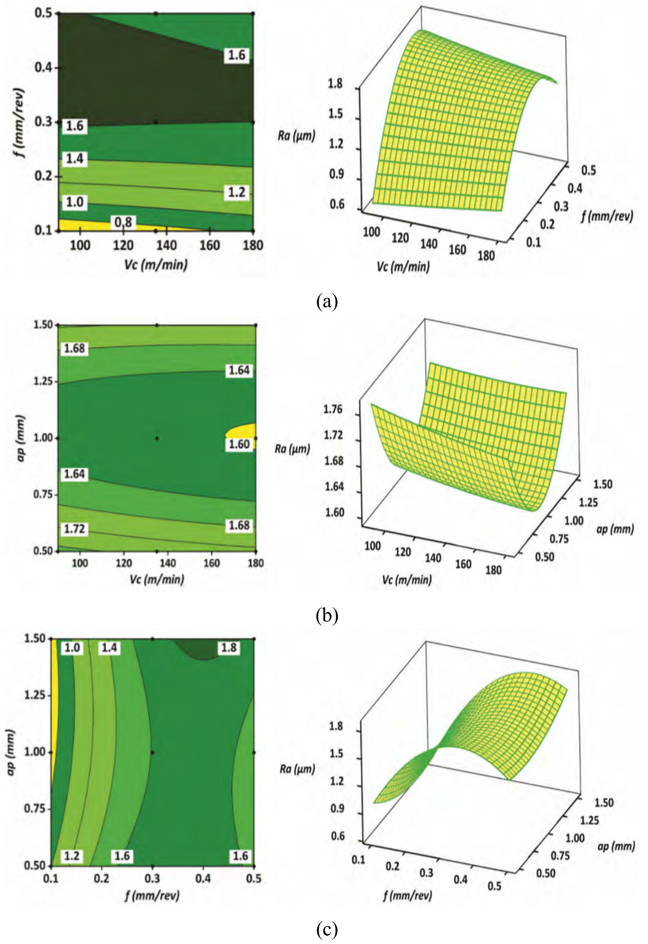

FIGURE 10. Contour plots and 3D surface plots for the estimated R_a with the expected ranges of (a) $0.6495 \le R_a \le 0.8596$, (b) $1.5983 \le R_a \le 1.6009$ and (c) $0.6994 \le R_a \le 0.8019$.

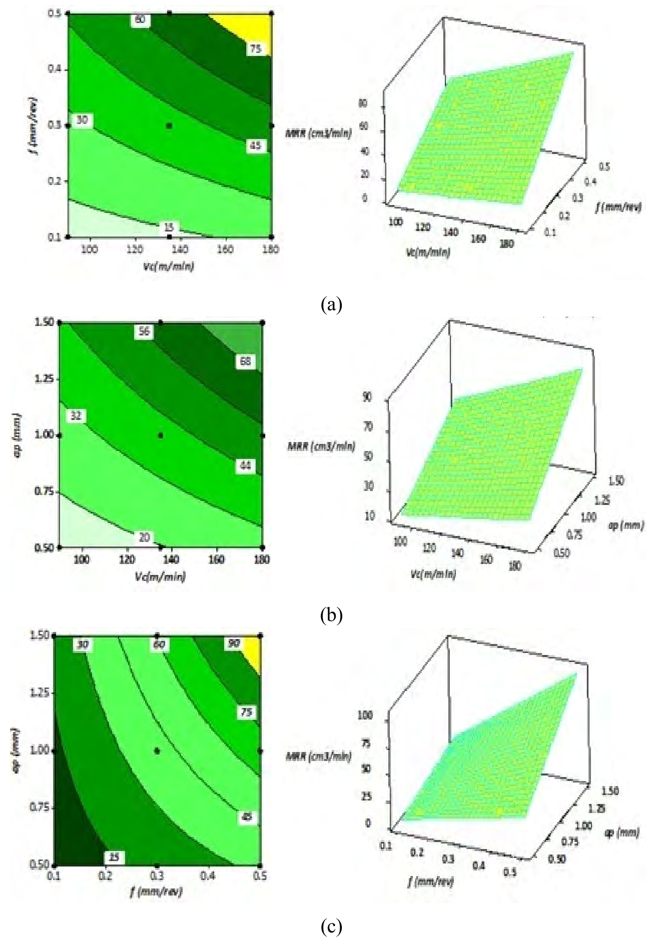

FIGURE 11. Contour plots and 3D surface plots for the estimated *MRR* with the expected ranges of (a) $75.2043 \le MRR \le 88.7093$, (b) $80 \le MRR \le 135$ and (c) $90.4712 \le MRR \le 102.295$.

concluded that the feed rate f is more significant in obtaining the high surface finish R_a for the selected material.

Figure 11(a) shows the effect of V_c and f on *MRR* when *ap* is held constant. It shows that the increase in V_c and f leads to maximum *MRR* which varies from $75.2043 \le MRR \le 88.7093\ cm^3/minute$. Figure 11(b) shows that the effect of V_c and *ap* on *MRR* when f is constant. The increase of V_c and *ap* leads to increase in *MRR* in the range of $80 \le MRR \le 135\ cm^3/minute$. Figure 11(c) shows the effects of f and *ap* on *MRR* when V_c is constant. The increase in f and *ap* increases *MRR*in the range of $90.4712 \le MRR \le 102.295\ cm^3/minute$. It is concluded that the highest value of V_c, f and *ap* are significant in obtaining higher *MRR* of Delrin material.

2) ANOVA RESULTS

Tables 5 and 6 present the ANOVA results of R_a and *MRR*, respectively, with 95% confidence interval It is observed that the components of V_c, V_c^2 and $V_c \times ap$ are found to be insignificant in modeling surface finish, while V_c^2, f^2 and ap^2 are the insignificant parameters of material removal rate. The higher contribution is given by feed rate with 55.69%, followed by f^2 with 31.05% in modeling the surface finish. Other terms such as linear term *ap* contributes with 3.16%, squared term ap^2 with 2.01%, interaction term $f \times ap$ with 3.62% and interaction term $V_c \times f$ with 2.07%. For *MRR*, the linear terms and interactive terms are significant, while the squared terms are found insignificant with contribution lesser than 1%. The linear terms V_c, f and *ap* have significant contribution of 13.93%, 46.30% and 26.89% respectively. The next term with high contribution is $f \times ap$ with 7.45%. The remaining interaction terms of $V_c \times f$ and $V_c \times ap$ have contribution of 2.88% and 2.09 % respectively.

B. PERFORMANCE EVALUATION OF EMOTLBO IN PROPOSED MACHINING PROBLEM

1) SIMULATION AND EXPERIMENTAL SETTINGS

The performance of EMOTLBO is compared with six well-established algorithms, i.e., non-dominated sorting genetic algorithm II (NSGA-II) [46], multi-objective particle swarm optimization (MOPSO) [48], multi-objective teaching-learning based optimization (MOTLBO) [29], multi-objective improved teaching-learning based optimization (MO-ITLBO) [34]–[36], multi-objective gray wolf optimizer (MOGWO) [49] and multi-objective sequential

TABLE 5. ANOVA results for surface roughness R_A.

Source	Degree of Freedom	Sequential Sum of Squares	Adjusted Sum of Squares	Adjusted Mean Squares	F-Value	P-Value	Contribution (%)	Remarks
Model	9	4.442	4.442	0.494	32.94	0.000		Significant
V_c	1	0.004	0.002	0.002	0.12	0.734	0.08	Insignificant
f	1	2.615	1.434	1.434	95.7	0.000	55.69	Significant
ap	1	0.008	0.148	0.148	9.9	0.006	0.17	Significant
V_c^2	1	0.000	0.000	0.000	0.01	0.939	0	Insignificant
f^2	1	1.458	1.401	1.401	93.5	0.000	31.04	Significant
ap^2	1	0.083	0.094	0.094	6.3	0.022	1.77	Significant
$V_c \times f$	1	0.097	0.120	0.120	8.01	0.012	2.07	Significant
$V_c \times ap$	1	0.006	0.001	0.001	0.07	0.801	0.13	Insignificant
$f \times ap$	1	0.170	0.170	0.170	11.33	0.004	3.62	Significant
Residual	17	0.255	0.255	0.015				
Total	26	4.696						
R^2 = 94.58%			R^2(Predicted) = 86.46%				R^2(Adjusted) = 91.71%	

TABLE 6. ANOVA results for surface roughness *MRR*.

Source	Degree of Freedom	Sequential Sum of Squares	Adjusted Sum of Squares	Adjusted Mean Squares	F-Value	P-Value	Contribution (%)	Remarks
Model	9	30,446.900	30,446.900	3,382.990	464.4	0.00		Significant
V_c	1	4,257.900	37.000	36.980	5.08	0.038	13.93	Significant
f	1	14,153.100	278.800	278.760	38.27	0.000	46.30	Significant
ap	1	8,221.700	113.200	113.200	15.54	0.001	26.89	Significant
V_c^2	1	2.000	2.400	2.390	0.33	0.574	0.01	Insignificant
f^2	1	7.600	0.900	0.900	0.12	0.729	0.02	Insignificant
ap^2	1	7.700	0.900	0.900	0.12	0.729	0.03	Insignificant
$V_c \times f$	1	880.900	713.300	713.330	97.92	0.000	2.88	Significant
$V_c \times ap$	1	639.000	378.800	378.780	52.01	0.000	2.09	Significant
$f \times ap$	1	2,277.000	2,277.000	2,277.020	312.58	0.000	7.45	Significant
Residual	17	123.800	123.800	7.280				
Total	26	30,570.80						
R^2 = 99.59%			R^2(Predicted) = 98.37%				R^2(Adjusted) = 99.38%	

TABLE 7. The parameter settings of all compared algorithms.

Algorithms	Parameter Settings
NSGA-II	$N \in \{20,30,40\}$, $P_{cr} = 0.9$, $P_{mut} = 1/D$
MOPSO	$N, \lvert A \rvert \in \{20,30,40\}$, $\omega \in 0.9 \to 0.4$, $c_1 = c_2 = 2.05$, $P_{mut} = 1/D$, $\alpha = 0.1$, $nGrid = 10$
MOTLBO	$N \in \{20,30,40\}$, $T_f \in [1,2]$
MO-ITLBO	$N, \lvert A \rvert \in \{20,30,40\}$, $nGroup = 4$, $T_f \in [1,2]$, $\varepsilon = 0.007$
MOGWO	$N, \lvert A \rvert \in \{20,30,40\}$, $\alpha = 0.1$, $nGrid = 10$
MOSQP	No specific parameters are required
EMOTLBO	$N, \lvert A \rvert \in \{20,30,40\}$, $P_{mut} = 1/D$, $\alpha = 0.1$, $nGrid = 10$

quadratic programming (MOSQP) [50]. Previous studies demonstrated the robustness of these six algorithms in tackling different types of MOPs. The performance of EMOTLBO with those six selected algorithms is anticipated to produce convincible results.

The parameter settings used in those algorithms by their respective authors are presented in Table 7. The crossover rate of NSGA-II was set as $P_{cr} = 0.9$, while the teaching factor T_f of MOTLBO and MO-ITLBO was randomly generated between 1 and 2. For MOPSO, the inertia weight ω was linearly decreased from 0.9 to 0.4, while the cognitive and social coefficients were set as $c_1 = c_2 = 2.05$. For MO-ITLBO, the multiple group learning approach was incorporated into teaching phase, and ε-dominance method of [20] was used to manage the archive. The number of groups denoted as *nGroup* and the value of ε were set as 4 and 0.007, respectively [37]. The implementation of MO-ITLBO was based on variant I proposed in [37] because it provides better clarity than [34]–[36]. No specific parameter setting is required for MOSQP and its source code is available in [51]. The same values were used for parameters of EMOTLBO common with other algorithms for the sake of fair comparison. For instance, the common parameters such as grid inflation coefficient and number of grid per dimension of MOPSO, MOGWO and EMOTLBO were set as $\alpha = 0.1$ and $nGrid = 10$, respectively. The maximum archive size A of these three algorithms were set equal to the population size. Mutation rates of NSGA-II, MOPSO and EMOTLBO were set as $p_{mut} = 1/D$, where D refers to the number of decision variables involved [46], [48].

The effect of population size on the search performance of all compared algorithms were studied by varying population size as $N = 20$, 30 and 40. The maximum number of fitness evaluation was used as termination condition for all algorithms and it was set as $FEs = 20{,}000$ for all population sizes. All algorithms were run 20 times independently using Matlab 2017a on the personal computer with Intel ®Core i7-7500 CPU @ 2.70GHz.

TABLE 8. The mean and standard deviation of coverage metric produced by all compared algorithms for different population sizes.

Compared Sets	$N = 20$		$N = 30$		$N = 40$	
	Mean	SD	Mean	SD	Mean	SD
$C(R_P, S_P)$	0.095	0.075	0.067	0.046	0.063	0.066
$C(S_P, R_P)$	0.013	0.018	0.042	0.048	0.019	0.029
$C(R_P, T_P)$	0.148	0.072	0.105	0.063	0.138	0.055
$C(T_P, R_P)$	0.005	0.016	0.020	0.033	0.004	0.012
$C(R_P, U_P)$	0.185	0.079	0.172	0.076	0.151	0.078
$C(U_P, R_P)$	0.000	0.000	0.013	0.023	0.004	0.012
$C(R_P, V_P)$	0.256	0.163	0.363	0.184	0.250	0.131
$C(V_P, R_P)$	0.015	0.024	0.003	0.010	0.008	0.018
$C(R_P, W_P)$	0.163	0.106	0.152	0.098	0.168	0.095
$C(W_P, R_P)$	0.038	0.029	0.042	0.024	0.024	0.027
$C(R_P, X_P)$	0.005	0.015	0.029	0.029	0.010	0.020
$C(X_P, R_P)$	0.000	0.000	0.000	0.000	0.000	0.000

Note: The Pareto non-dominated solution sets produced by EMOTLBO, NSGA-II, MOPSO, MOTLBO, MO-ITLBO, MOGWO and MOSQP algorithms are denoted as R_P, S_P, T_P, U_P, V_P, W_p and X_p respectively.

2) RESULTS AND DISCUSSIONS

The mean and standard deviation (SD) of coverage metric obtained by all compared algorithms in 30 independent runs for the population sizes of 20, 30 and 40 are presented in Table 8. It is observed that EMOTLBO delivers the best performance in all population sizes because it produces higher percentages of non-dominated solutions to dominate the solution sets obtained by other peers. For instance, 36.3% of non-dominated solutions produced by the MO-ITLBO are dominated by those of EMOTLBO when $N = 30$, while only 0.3% of non-dominated solutions produced by EMOTLBO is dominated by those of MO-ITLBO. For $N = 40$, there are 13.8% and 15.1% of non-dominated solutions produced by MOPSO and MOTLBO, respectively, are dominated by the solution sets of EMOTLBO. Nevertheless, only 0.4% of the non-dominated solutions obtained by EMTLBO is dominated by those of MOPSO and MOTLBO. Among all of the six algorithms in benchmarking, MOSQP has demonstrated the most competitive performance as more than 1.5% of its non-dominated solutions are inferior to the Pareto-front of EMOTLBO. On the other hand, none of the non-dominated solutions produced by EMOTLBO is inferior to those of MOSQP for all population sizes.

TABLE 9. The mean and standard deviation of spacing metric produced by all compared algorithms for different population sizes.

Algorithms	$N = 20$		$N = 30$		$N = 40$	
	Mean	SD	Mean	SD	Mean	SD
NSGA-II	1.267	1.041	1.612	1.383	1.548	1.434
MOPSO	3.758	1.949	3.095	1.514	4.001	2.188
MOTLBO	1.999	1.878	2.883	1.606	2.952	2.214
MO-ITLBO	0.703	0.304	0.890	0.499	0.673	0.275
MOGWO	2.741	2.024	2.632	1.003	3.260	1.943
MOSQP	6.133	0.000	10.309	0.000	12.488	0.000
EMOTLBO	0.592	0.572	0.813	0.967	0.512	0.412

Table 9 presents the mean and SD values of spacing metric produced by all algorithms in the same 20 independent runs for the population sizes of 20, 30 and 40. It is observed that the spacing value of Pareto-fronts obtained using EMOTLBO is the lowest as compared to those of NSGA-II, MOPSO, MOTLBO, MO-ITLBO, MOGWO and MOSQP. This implies that the proposed EMOTLBO can generate Pareto-fronts with more uniform distribution. Though EMOTLO, MOPSO and MOGWO used similar external archive concept to store the non-dominated solutions obtained, simulation results have proved that the archive updating strategy of EMOTLBO is more efficient in eliminating the duplicated solutions based on the crowding distance of archive members.

In contrary, the probabilistic selection method used by MOPSO and MWGWO to exclude the redundant archive members are less efficient because there is a narrow chance to accidentally remove the less dense members from archive. Notable observations were demonstrated by MO-ITLBO and MOSQP for producing the second lowest and largest values of spacing metrics, respectively. The Pareto-front of MOSQP is not uniformly distributed in spite of better quality solutions generated. Although MO-ITLBO produced Pareto-front with better distribution, it seems many generated solutions are inferior. As compared with these two algorithms, the proposed EMOTBLO has demonstrated more competitive performance in terms of well distributed Pareto-front with better solutions.

Figure 12 shows the Pareto-fronts produced by NSGA-II, MOPSO, MOTLBO, MO-ITLBO, MOGWO, MOSQP and EMOTLBO for $N = 40$. Significant discontinuities are found on the Pareto-fronts of NSGA-II, MOPSO, MOGWO and MOSQP, implying that these algorithms tend to be trapped into the local Pareto-front and cannot approach the true Pareto-front effectively. These justify the presence of inferior non-dominated solutions generated by NSGA-II, MOPSO, MOGWO and MOSQP when compared to EMOTLBO. In addition, the non-dominated solutions stored in Pareto front of EMOTLBO is the most uniformly distributed as compared to all of its six competitors. The qualitative results presented in Figure 12 are consistent with the quantitative results of Tables 8 and 9.

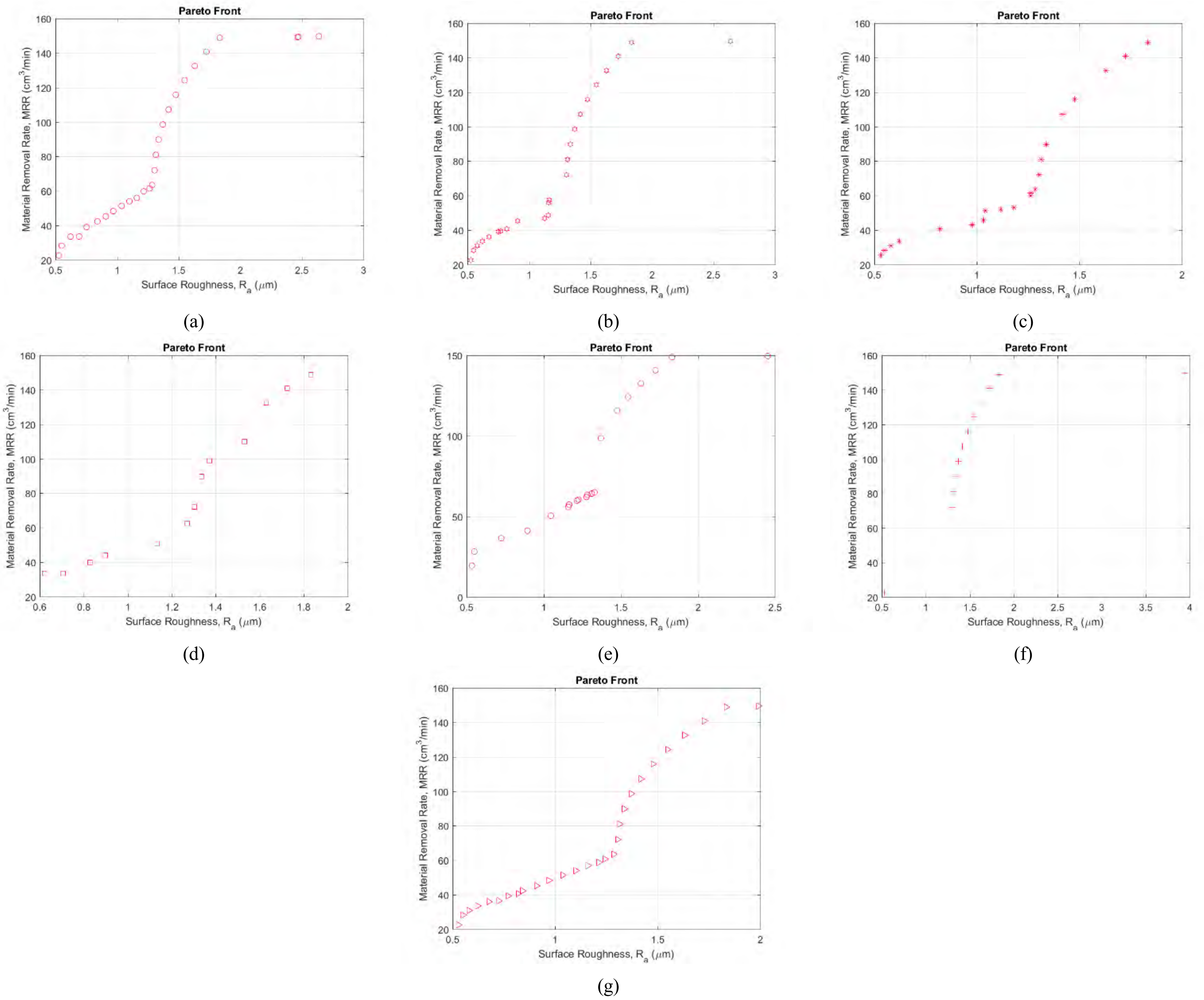

FIGURE 12. The Pareto-fronts produced by (a) NSGA-II, (b) MOPSO, (c) MOTLBO, (d) MO-ITLBO, (e) MOGWO, (f) MOSQP and (g) EMOTLBO.

TABLE 10. Comparison between the predicted and experimental values.

Machining Condition		$w_1 = 0.5$, $w_2 = 0.5$
Machining Parameters	Cutting speed, V_c	200
	Feed rate, f	0.5
	Depth of cut, ap	1.4
Predicted Values	Surface finish, R_a	1.6299
	Material removal rate, MRR	132.5714
Experimental Values	Surface finish, R_a	1.69
	Material removal rate, MRR	138.5
Error Rates	ΔR_a (%)	3.556
	ΔMRR (%)	4.281

Apart from evaluating the quality of Pareto-fronts produced by EMOTLBO, it is also essential to validate the optimum machining parameters produced by EMOTLBO based on the relative importance of objectives with experimental values of surface roughness R_a and material removal rate MRR. Let w_1 and w_2 be the weight values that indicating the importance level of objectives to minimize R_a and maximize MRR, respectively, where $w_1 + w_2 = 1$. Since both objectives of minimizing R_a and maximizing MRR are contradicting with each other, the weightage setting of $w_1 = w_2 = 0.5$ are considered in this section in order to give equal importance in producing the products with maximum quality and maximum quantity simultaneously during the machining process.

An EMOTLBO with population size of $N = 40$ was executed to obtain the Pareto-front as illustrated in Figure 12(g). Based on the importance levels of both objectives as represented by w_1 and w_2, fuzzy decision maker was used to select the unique optimum solution corresponding to each machining condition using (15)-(17). The predicted optimum machining parameters and experimental values of R_a and MRR and their errors are presented in Table 10.

TABLE 11. 12 test functions used in comprehensive simulation study.

Problem	Mathematical Formulation
ZDT1	$f_1(x)=x_1$, $f_2(x)=g(x)\left(1-\sqrt{x_1/g(x)}\right)$, $g(x)=1+\frac{9}{D-1}\sum_{i=2}^{D}x_i$, $D=30$, $0\le x_i\le 1$, $i=1,2,...,D.$
ZDT2	$f_1(x)=x_1$, $f_2(x)=g(x)\left(1-\left(x_1/g(x)\right)^2\right)$, $g(x)=1+\frac{9}{D-1}\sum_{i=2}^{D}x_i$, $D=30$, $0\le x_i\le 1$, $i=1,2,...,D.$
ZDT3	$f_1(x)=x_1$, $f_2(x)=g(x)\left(1-\sqrt{x_1/g(x)}-\frac{x_1}{g(x)}\sin(10\pi x_1)\right)$, $g(x)=1+\frac{9}{D-1}\sum_{i=2}^{D}x_i$, $D=30$, $0\le x_i\le 1$, $i=1,2,...,D.$
ZDT4	$f_1(x)=x_1$, $f_2(x)=g(x)\left(1-\sqrt{x_1/g(x)}\right)$, $g(x)=1+10(n-1)+\sum_{i=2}^{D}\left(x_i^2-10\cos(4\pi x_i)\right)$, $D=10$, $0\le x_1\le 1$, $-5\le x_i\le 5$, $i=2,3,...,D.$
ZDT6	$f_1(x)=1-e^{-4x_1}\sin^6(6\pi x_1)$, $f_2(x)=g(x)\left(1-\left(x_1/g(x)\right)^2\right)$, $g(x)=1+9\left(\left(\sum_{i=2}^{D}x_i\right)\Big/(D-1)\right)^{0.25}$, $D=10$, $0\le x_i\le 1$, $i=1,2,...,D.$
DLTZ1	$f_1(x)=\frac{1}{2}x_1x_2(1+g(x))$, $f_2(x)=\frac{1}{2}x_1(1-x_2)(1+g(x))$, $f_3(x)=\frac{1}{2}(1-x_1)(1+g(x))$, $g(x)=100\left[(n-3+1)+\sum_{i=3}^{D}\left((x_i-0.5)^2-\cos\left(20\pi(x_i-0.5)\right)\right)\right]$, $D=7$, $0\le x_i\le 1$, $i=1,2,...,D.$
DLTZ2	$f_1(x)=(1+g(x))\cos(0.5\pi x_1)\cos(0.5\pi x_2)$, $f_2(x)=(1+g(x))\cos(0.5\pi x_1)\sin(0.5\pi x_2)$, $f_3(x)=(1+g(x))\sin(0.5\pi x_1)$, $g(x)=\sum_{i=3}^{D}(x_i-0.5)^2$, $D=12$, $0\le x_i\le 1$, $i=1,2,...,D.$
DLTZ3	$f_1(x)=(1+g(x))\cos(0.5\pi x_1)\cos(0.5\pi x_2)$, $f_2(x)=(1+g(x))\cos(0.5\pi x_1)\sin(0.5\pi x_2)$, $f_3(x)=(1+g(x))\sin(0.5\pi x_1)$, $g(x)=100\left[(D-3+1)+\sum_{i=3}^{D}\left((x_i-0.5)^2-\cos\left(20\pi(x_i-0.5)\right)\right)\right]$, $D=12$, $0\le x_i\le 1$, $i=1,2,...,D.$
DLTZ4	$f_1(x)=(1+g(x))\cos(0.5\pi x_1^{\alpha})\cos(0.5\pi x_2^{\alpha})$, $f_2(x)=(1+g(x))\cos(0.5\pi x_1^{\alpha})\sin(0.5\pi x_2^{\alpha})$, $f_3(x)=(1+g(x))\sin(0.5\pi x_1^{\alpha})$, $g(x)=\sum_{i=3}^{D}(x_i-0.5)^2$, $\alpha=100$, $D=12$, $0\le x_i\le 1$, $i=1,2,...,D.$
DLTZ5	$f_1(x)=(1+g(x))\cos(0.5\pi\theta_1)\cos(0.5\pi\theta_2)$, $f_2(x)=(1+g(x))\cos(0.5\pi\theta_1)\sin(0.5\pi\theta_2)$, $f_3(x)=(1+g(x))\sin(0.5\pi\theta_1)$, $g(x)=\sum_{i=3}^{D}(x_i-0.5)^2$, $\theta_1=x_1$, $\theta_2=\frac{(1+2x_2g(x))}{2(1+g(x))}$, $D=12$, $0\le x_i\le 1$, $i=1,2,...,D.$
DLTZ6	$f_1(x)=(1+g(x))\cos(0.5\pi\theta_1)\cos(0.5\pi\theta_2)$, $f_2(x)=(1+g(x))\cos(0.5\pi\theta_1)\sin(0.5\pi\theta_2)$, $f_3(x)=(1+g(x))\sin(0.5\pi\theta_1)$, $g(x)=\sum_{i=3}^{D}x_i^{0.1}$, $\theta_1=x_1$, $\theta_2=\frac{(1+2x_2g(x))}{2(1+g(x))}$, $D=12$, $0\le x_i\le 1$, $i=1,2,...,D.$
DLTZ7	$f_1(x)=x_1$, $f_2(x)=x_2$, $f_3(x)=(1+g(x))\left(3-\frac{f_1(x)}{1+g(x)}\left(1+\sin(3\pi f_1(x))\right)-\frac{f_2(x)}{1+g(x)}\left(1+\sin(3\pi f_2(x))\right)\right)$, $g(x)=1+\frac{9}{D-3}\sum_{i=3}^{D}x_i$, $D=12$, $0\le x_i\le 1$, $i=1,2,...,D.$

For the optimum parameters of $V_c = 200$ *m/minute*, $f = 0.50$ *mm/rev* and $ap = 1.2mm$, predicted values of $R_a = 1.6299$ μm and $MRR = 132.5714$ cm^3*/minute* is obtained from simulation with the relative importance of $w_1 = 0.5$ and $w_2 = 0.5$, respectively.

From the validation results shown in Table 10, 3.556 % and 4.281% of error are noticed between the experimental and predicted values of R_a and MRR, respectively. With these significantly small error rates, it is concluded that there is a good agreement between the simulation results and the experimental results.

C. PERFORMANCE EVALUATION OF EMOTLBO IN TEST FUNCTIONS

1) TEST FUNCTIONS AND PERFORMANCE METRIC

Apart from the proposed Delrin machining problem, another 12 test functions characterized with convexity, concavity, discontinuity or the presence of local Pareto-fronts were also employed to evaluate the general optimization performance of proposed EMOTLBO. These benchmark problems are classified into two categories, i.e., the high-dimensional bi-objective problems covering ZDT1-ZDT4 and ZDT6 [47], and the scalable objective problems composed of DLTZ1-DLTZ7 [52]. The mathematical description of these 12 test functions are presented in Table 11.

In contrary to Delrin machining problem, the true Pareto-fronts of these 12 test functions are available in advance. Hence, the inverted generation distance (IGD) metric [53] can be used to assess the optimization performance of EMOTLBO in terms of its capability to generate the non-dominated solution sets that are not only uniformly distributed in objective space, but also can approximate the true Pareto-fronts as close as possible. Assume that A is the approximated solution set obtained by a particular

TABLE 12. IGD results on the ZDT and DTZ problems.

Problem		Algorithms					
		NSGA-II	MOPSO	MOTLBO	MO-ITLBO	MOGWO	EMOTLBO
ZDT1	Mean	1.52E-03	*5.05E-04*	6.10E-04	2.05E-03	7.41E-03	**2.03E-04**
	SD	2.16E-04	5.88E-05	9.26E-05	2.27E-04	2.49E-03	1.10E-06
	h	+	+	+	+	+	
ZDT2	Mean	*1.69E-03*	2.18E-02	1.50E-02	3.12E-02	3.17E-02	**2.10E-04**
	SD	3.57E-04	2.67E-02	1.64E-02	6.79E-03	4.49E-03	2.24E-06
	h	+	+	+	+	+	
ZDT3	Mean	2.87E-03	*5.92E-04*	9.10E-04	2.82E-03	2.28E-03	**2.40E-04**
	SD	2.09E-03	9.43E-05	1.99E-04	3.17E-04	7.60E-04	9.57E-07
	h	+	+	+	+	+	
ZDT4	Mean	*4.45E-03*	5.13E-01	1.80E-01	1.26E-01	1.30E-01	**2.87E-03**
	SD	5.33E-03	4.54E-01	7.06E-02	1.02E-01	9.75E-02	2.09E-03
	h	=	+	+	+	+	
ZDT6	Mean	1.35E-03	*4.68E-04*	6.37E-04	1.71E-03	4.80E-03	**1.65E-04**
	SD	3.09E-04	8.27E-05	1.31E-04	2.68E-04	4.30E-03	1.90E-06
	h	+	+	+	+	+	
DLTZ1	Mean	**5.01E-04**	2.48E-01	2.77E-01	2.46E-01	1.84E-01	*3.39E-03*
	SD	2.34E-03	3.51E-02	3.40E-02	2.46E-01	6.55E-02	3.05E-05
	h	-	+	+	+	+	
DLTZ2	Mean	*2.43E-03*	2.88E-03	2.23E-03	2.62E-03	5.46E-03	**1.85E-03**
	SD	1.65E-04	9.98E-04	1.16E-04	3.09E-04	5.81E-04	4.45E-05
	h	+	+	+	+	+	
DLTZ3	Mean	**1.11E-01**	2.44E+00	*2.29E+00*	2.71E+00	2.74E+00	2.57E+00
	SD	6.18E-02	1.51E-01	1.42E-01	2.44E-01	5.73E-01	1.24E-01
	h	-	-	=	+	+	
DLTZ4	Mean	1.15E-02	*5.18E-03*	7.18E-03	6.79E-03	**4.35E-03**	5.61E-03
	SD	3.78E-03	3.39E-03	2.00E-03	2.28E-03	4.86E-03	5.74E-04
	h	+	=	+	+	-	
DLTZ5	Mean	5.97E-04	*6.85E-04*	9.46E-04	2.51E-03	1.19E-03	**5.55E-04**
	SD	5.00E-05	2.25E-04	1.27E-04	4.06E-04	4.66E-04	5.26E-05
	h	+	+	+	+	+	
DLTZ6	Mean	5.59E-04	*1.88E-04*	2.25E-04	6.79E-04	1.23E-03	**8.49E-05**
	SD	7.40E-05	2.29E-05	3.31E-05	3.86E-05	6.54E-04	2.37E-06
	h	+	+	+	+	+	
DLTZ7	Mean	5.21E-03	*9.52E-04*	**9.18E-04**	5.28E-03	1.39E-02	9.66E-04
	SD	3.50E-03	7.00E-05	4.20E-05	6.90E-03	6.33E-03	4.53E-05
	h	+	=	-	+	+	
	#BM	2	0	1	0	1	8
	w/t/l	10/0/2	9/0/3	10/0/2	12/0/0	11/0/1	
	+/=/-	9/1/2	9/2/1	10/1/1	12/0/0	11/0/1	

multi-objective optimization algorithm, while TP^* is a set of uniformly distributed solutions acquired from true Pareto-front. Let $|TP^*|$ represents the number of solutions in the true Pareto-front TP^* and $\Psi\left(TP_i^*, A\right)$ be an operator to return the minimum Euclidean distance from the i-th member of TP^* to the approximated solutions of A in objective space. Then, the IGD value of TP^* to A is defined as [53]:

$$IGD\left(A, TP^*\right) = \frac{\sum_{i=1}^{|TP^*|} \Psi\left(TP_i^*, A\right)}{|TP^*|} \tag{22}$$

If $|TP^*|$ is sufficiently large to represent the true Pareto-front, both of the diversity and convergence of the approximated set A can be measured using $IGD\left(A, TP^*\right)$. Smaller value of $IGD\left(A, TP^*\right)$ is more desirable because it implies that the approximated solution set A produced is more evenly distributed and closer to the true Pareto-front TP^*.

A non-parametric statistical procedure known as Wilcoxon test was also employed for rigorous performance comparison between EMOTLBO and its peers to ensure the better results achieved by the best algorithm is statistically significant instead of by chance [54]. In this study, the pairwise comparison between EMOTLBO and its peers were conducted at 5% significant level, i.e., $\sigma = 0.05$. The h value produced by Wilcoxon test can determine if EMOTLBO is statistically better (i.e., h = '+'), insignificant (i.e., h = '=') or worse (i.e., h = '−') than its peers.

The optimization performances of EMOTLBO in solving all 12 test functions were compared with those of NSGA-II, MOPSO, MOTLBO, MO-ITLBO and MOGWO. Similar parameter settings as presented in Table 12 are adopted for all involved algorithms except for the population size N and archive size $|A|$. Specifically, the values of N and $|A|$ are set as 100 in these algorithms were used to solve the bi-objective problems (ZDT1-ZDT4 and ZDT6), while $N = |A| = 150$ were assigned to the algorithms when dealing with the tri-objective problems of DLTZ1-DLTZ7 [34]. For each test function, the maximum fitness evaluation number was set as 300,000 and each compared algorithm is executed for 30 times.

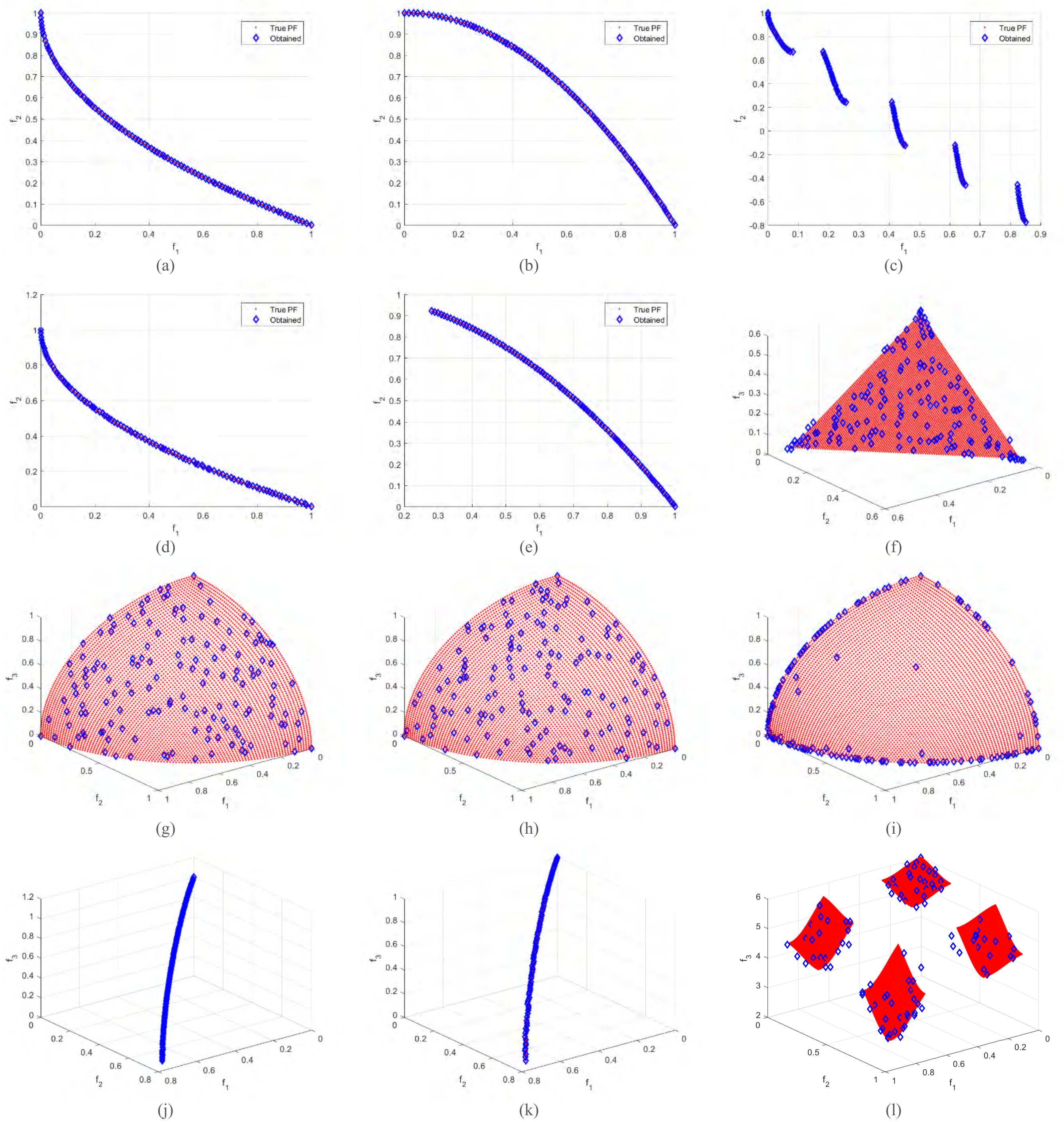

FIGURE 13. The plots of best performance obtained by EMOTLBO on (a) ZDT1, (b) ZDT2, (c) ZDT3, (d) ZDT4, (e) ZDT6, (f) DTLZ1, (g) DTLZ2, (h) DTLZ3, (i) DTLZ4, (j) DTLZ5, (k) DTLZ6 and (l) DTLZ7.

2) COMPARISONS OF EMOTLBO WITH OTHER MULTI-OBJECTIVE OPTIMIZATION ALGORITHMS

The comparison results of mean IGD (IGD_{mean}), standard deviation (SD) and Wilcoxon test produced by all compared algorithms in each test function are presented in Table 12, where the best and second best results are indicated with boldface and underline texts, respectively. The comparison of IGD_{mean} values between the EMOTLBO and its peers are summarized as $w/t/l$ and #BM, where $w/t/l$ means that EMOTLBO outperforms a given peer in w functions, ties in t functions and loses in l functions. #BM refers to the number of best (i.e., lowest) IGD_{mean} achieved by each algorithm.

The Wilcoxon test result denoted as h is summarized as $+/=/-$ to indicate the number of test functions in which EMOTLBO performs significantly better, almost the same and significant worse than its competitor, respectively.

Table 12 shows the proposed EMOTLBO has produced the lowest IGD_{mean} values in eight test functions except for DLTZ1, DLTZ3, DLTZ4 and DLTZ7 which are dominated by NSGA-II, MOTLBO and MOGWO. This implies that the non-dominated solution sets generated by EMOTLBO in most of test functions are uniformly distributed in objective space and can closely approximate the true Pareto-fronts of each respective function. From Table 12, it is notable that some compared algorithms lack of capabilities in handling the test functions with certain characteristics. For example, NAGA-II cannot effectively approach to the true Pareto-front of ZDT1, ZDT3, ZDT6 and DLTZ4 although it performs relatively well in the other eight test functions. Meanwhile, the MOPSO can handle ZDT1, ZDT3, ZDT6, DLTZ4, DLTZ5, DLTZ6 and DLTZ7 quite well but it fails to produce good approximation of true Pareto-front for the remaining five test functions. Compare to both MOTLBO and MO-ITLBO, the optimization capability of EMOTLBO has been improved significantly. The inclusion of mutation mechanism prevents the trapping of non-dominated solutions found in local Pareto-fronts, while the proposed archive controller delete the most crowded archive members, hence able to ensure the approximated solution sets produced by the EMOTLBO are more uniformly distributed.

Similar observations were found from Wilcoxon test result in which the IGD_{mean} values produced by EMOTLBO are significantly better than the other five algorithms in majority of test functions. This implies that the excellent optimization performance delivered by EMOTLBO in solving most test functions are statistically significant and not achieved by any random chances. Table 12 shows that no significant difference between the IGD_{mean} results obtained by NSGA-II and EMOTLBO in ZDT4. Similar observations can be found in DLTZ3 (MOTLBO vs EMOTLBO), DLTZ4 (MOPSO vs EMOTLBO) and DLTZ7 (MOPSO vs EMOTLBO).

Finally, the best results of EMOTLBO in solving all 12 test functions are also visually illustrated in Figure 13, where the true Pareto-fronts of each test function are plotted with red lines, while the approximated Pareto-fronts generated by EMOTLBO are marked with blue diamond. The qualitative analyses shown in Figure 13 are consistent with the quantitative analyses tabulated in Table 12 because the non-dominated solution sets found by EMOTLBO in majority of test functions are distributed uniformly and able to approach the respective true Pareto-front effectively.

V. CONCLUSION

The aim of this research is to find the optimum machining conditions to simultaneously achieve minimum surface roughness and maximum material removal rate during the turning of Delrin. A three-level L_{27} orthogonal matrix was first formulated and experiments were conducted with Delrin specimens with 30 *mm* diameter. The Carbide tip (CNMG) cutting tool inserted with a tool angle of 80° and servo super cut coolant 32 was used for turning three steps of equal length of 10 *mm*. The RSM model was rendered from the experimental data and the model was further verified using ANOVA. The R^2 value for surface roughness R_a was found to be 94.58%, implying that the predicted values are close to the experimental counterparts. The adequacy and practical applicability of the model within the expected range of values are also confirmed. Based on these experimentally developed regression models, two objective functions to be considered in the multi-objective machining optimization problem of Delrin material are derived.

Apart from deriving the regression models of Delrin, an improved multi-objective optimization algorithm known as EMOTLBO was proposed to solve multiobjective problem. Several modifications were incorporated into EMOTLBO, including: (i) an archive used to store non-dominated solutions, (ii) an archive controller to manage the non-dominated solutions, (iii) a new selection mechanisms for teacher and peer learner (iv) a mutation operator that emulates brainstorming session in classroom to prevent premature convergence and (v) a fuzzy decision maker to softly select the preferred non-dominated solution from Pareto front based on the importance of objectives. Extensive simulation studies reveal that EMOTLBO outperforms six well-established multi-objective optimization algorithms for being able to produce the more evenly distributed Pareto fronts and higher number of non-dominated solutions. The simulation results of EMOTLBO were validated and observed only $<5\%$ of error for both surface roughness and material removal rate, implying that the good agreement between the simulation and experimental results. Finally, the general optimization capability of EMOTLBO was proven for being able to deliver competitive performance in solving the 12 standard test functions with different characteristics. The non-dominated solution sets produced by EMOTLBO for each test function are not only uniformly distributed, but also close to the respective true Pareto-front.

REFERENCES

[1] A. Chabbi, M. A. Yallese, M. Nouioua, I. Meddour, T. Mabrouki, and F. Girardin, "Modeling and optimization of turning process parameters during the cutting of polymer (POM C) based on RSM, ANN, and DF methods," *Int. J. Adv. Manuf. Technol.*, vol. 91, nos. 5–8, pp. 2267–2290, Jul. 2017.

[2] M. Kaddeche, K. Chaoui, and M. A. Yallese, "Cutting parameters effects on the machining of two high density polyethylene pipes resins: Cutting parameters effects on HDPE machining," *Mech. Ind.*, vol. 13, no. 5, pp. 307–316, Dec. 2012.

[3] M. R. Panda, S. K. Biswal, and Y. K. Sharma, "Experimental analysis on the effect of process parameters during CNC turning on nylon-6/6 using tungsten carbide tool," *Int. J. Eng. Sci. Res. Technol.*, vol. 5, no. 4, pp. 79–84, Apr. 2016.

[4] D. Lazarević, M. Madić, P. Janković, and A. Lazarević, "Cutting parameters optimization for surface roughness in turning operation of polyethylene (PE) using Taguchi method," *Tribol. Ind.*, vol. 34, no. 2, pp. 68–73, Jan. 2012.

[5] N. Hamlaoui, S. Azzouz, K. Chaoui, Z. Azari, and M.-A. Yallese, "Machining of tough polyethylene pipe material: Surface roughness and cutting temperature optimization," *Int. J. Adv. Manuf. Technol.*, vol. 92, nos. 5–8, pp. 2231–2245, Sep. 2017.

[6] V. N. Gaitonde, S. R. Karnik, F. Mata, and J. P. Davim, "Taguchi approach for achieving better machinability in unreinforced and reinforced polyamides," *J. Reinforced Plastics Compos.*, vol. 27, no. 9, pp. 909–924, Jan. 2018.

[7] V. N. Gaitonde, S. R. Karnik, F. Mata, and J. P. Davim, "Study on some aspects of machinability in unreinforced and reinforced polyamides," *J. Compos. Mater.*, vol. 43, no. 7, pp. 725–739, Mar. 2009.

[8] J. L. C. Salles and M. T. T. Gonçalves, "Effects of machining parameters on surface quality of the ultra high molecular weight polyethylene (UHMWPE)," *Matéria*, vol. 8, no. 1, pp. 1–10, 2003.

[9] J. P. Davim, P. Reis, V. Lapa, and C. C. António, "Machinability study on polyetheretherketone (PEEK) unreinforced and reinforced (GF30) for applications in structural components," *Compos. Struct.*, vol. 62, no. 1, pp. 67–73, Oct. 2003.

[10] M. Rahman, S. Ramakrishna, and H. C. Thoo, "Machinability study of carbon/peek composites," *Mach. Sci. Technol.*, vol. 3, no. 1, pp. 49–59, Sep. 1998.

[11] J. A. Shukor, S. Said, R. Harun, S. Husin, and A. Kadir, "Optimising of machining parameters of plastic material using Taguchi method," *Adv. Mater. Process. Technol.*, vol. 2, no. 1, pp. 50–56, Feb. 2016.

[12] K. Palanikumar, L. Karunamoorthy, and R. Karthikeyan, "Assessment of factors influencing surface roughness on the machining of glass fiber-reinforced polymer composites," *Mater. Des.*, vol. 27, no. 10, pp. 862–871, Jun. 2005.

[13] M. Madić, V. Marinković, and M. Radovanović, "Mathematical modeling and optimization of surface roughness in turning of polyamide based on artificial neural network," *Proc. Mech.*, vol. 18, no. 5, pp. 2029–6983, Nov. 2012.

[14] I. Mukherjee and P. K. Ray, "A review of optimization techniques in metal cutting processes," *Comput. Ind. Eng.*, vol. 50, nos. 1–2, pp. 15–34, May 2006.

[15] M. Chandrasekaran, M. Muralidhar, C. M. Krishna, and U. S. Dixit, "Application of soft computing techniques in machining performance prediction and optimization: A literature review," *Int. J. Adv. Manuf. Technol.*, vol. 46, nos. 5–8, pp. 445–464, Jan. 2010.

[16] N. Yusup, A. M. Zain, and S. Z. M. Hashim, "Evolutionary techniques in optimizing machining parameters: Review and recent applications (2007–2011)," *Exprt Syst. Appl.*, vol. 39, no. 10, pp. 9909–9927, Aug. 2012.

[17] R. V. Rao and V. D. Kalyankar, "Optimization of modern machining processes using advanced optimization techniques: A review," *Int. J. Adv. Manuf. Technol.*, vol. 73, nos. 5–8, pp. 1159–1188, Jul. 2014.

[18] Y. Collette and P. Siarry, *Multiobjective Optimization: Principles and Case Studies*. Berlin, Germany: Springer-Verlag, Jan. 2003.

[19] A. T. Abbas, M. Aly, and K. Hamza, "Multiobjective optimization under uncertainty in advanced abrasive machining processes via a fuzzy-evolutionary approach," *J. Manuf. Sci. Eng.*, vol. 138, no. 7, pp. 071003-1–071003-9, Mar. 2016.

[20] K. Deb, M. Mohan, and S. Mishra, "Evaluating the ϵ-domination based multi-objective evolutionary algorithm for a quick computation of Pareto-optimal solutions," *Evol. Comput.*, vol. 13, no. 4, pp. 501–525, Dec. 2005.

[21] E. Zitzler, M. Laumanns, and L. Thiele, "SPEA2: Improving the strength Pareto evolutionary algorithm for multiobjective optimization," in *Proc. Evol. Methods Design Optim. Control Appl. Ind. Problems*, Athens, Greece, 2001, pp. 95–100.

[22] D. W. Corne, N. R. Jerram, J. D. Knowles, and M. J. Oates, "PESA-II: Region-based selection in evolutionary multiobjective optimization," in *Proc. 3rd Annu. Conf. Genet. Evol. Comput.*, 2001, pp. 283–290.

[23] Q. Zhang and H. Li, "MOEA/D: A multiobjective evolutionary algorithm based on decomposition," *IEEE Trans. Evol. Comput.*, vol. 11, no. 6, pp. 712–731, Dec. 2007.

[24] K. Deb and H. Jain, "An evolutionary many-objective optimization algorithm using reference-point-based nondominated sorting approach, part I: Solving problems with box constraints," *IEEE Trans. Evol. Comput.*, vol. 18, no. 4, pp. 577–601, Aug. 2014.

[25] R. Teimouri, H. Baseri, and R. Moharami, "Multi-responses optimization of ultrasonic machining process," *J. Intell. Manuf.*, vol. 26, no. 4, pp. 745–753, Aug. 2015.

[26] C. P. Mohanty, S. S. Mahapatra, and M. R. Singh, "A particle swarm approach for multi-objective optimization of electrical discharge machining process," *J. Intell. Manuf.*, vol. 27, no. 6, pp. 1171–1190, Dec. 2016.

[27] R. V. Rao, D. P. Rai, and J. Balic, "A multi-objective algorithm for optimization of modern machining processes," *Eng. Appl. Artif. Intell.*, vol. 61, pp. 103–125, May 2017.

[28] R. V. Rao, V. J. Savsani, and D. P. Vakharia, "Teaching–learning-based optimization: A novel method for constrained mechanical design optimization problems," *Comput.-Aided Des.*, vol. 43, no. 3, pp. 303–315, Mar. 2011.

[29] W. Lin *et al.*, "Multi-objective teaching–learning-based optimization algorithm for reducing carbon emissions and operation time in turning operations," *Eng. Optim.*, vol. 47, no. 7, pp. 994–1007, Jun. 2014.

[30] R. V. Rao, D. P. Rai, and J. Balic, "Multi-objective optimization of machining and micro-machining processes using non-dominated sorting teaching–learning-based optimization algorithm," *J. Intell. Manuf.*, pp. 1–23, 2016, doi: 10.1007/s10845-016-1210-5.

[31] D. Li, C. Zhang, X. Shao, and W. Lin, "A multi-objective TLBO algorithm for balancing two-sided assembly line with multiple constraints," *J. Intell. Manuf.*, vol. 27, no. 4, pp. 725–739, Aug. 2016.

[32] S. Sultana and P. K. Roy, "Multi-objective quasi-oppositional teaching learning based optimization for optimal location of distributed generator in radial distribution systems," *Int. J. Elect. Power Energy Syst.*, vol. 63, pp. 534–545, Dec. 2014.

[33] K. Yu, X. Wang, and Z. Wang, "Self-adaptive multi-objective teaching-learning-based optimization and its application in ethylene cracking furnace operation optimization," *Chemometrics Intell. Lab. Syst.*, vol. 146, pp. 198–210, Aug. 2015.

[34] R. V. Rao and V. Patel, "A multi-objective improved teaching-learning based optimization algorithm for unconstrained and constrained optimization problems," *Int. J. Ind. Eng. Comput.*, vol. 5, no. 1, pp. 1–22, 2014.

[35] V. K. Patel and V. J. Savsani, "A multi-objective improved teaching–learning based optimization algorithm (MO-ITLBO)," *Inf. Sci.*, vol. 357, pp. 182–200, Aug. 2016.

[36] R. V. Rao and G. G. Waghmare, "Multi-objective design optimization of a plate-fin heat sink using a teaching-learning-based optimization algorithm," *Appl. Therm. Eng.*, vol. 76, pp. 521–529, Feb. 2015.

[37] S. Chinta, R. Kommadath, and P. Kotecha, "A note on multi-objective improved teaching–learning based optimization algorithm (MO-ITLBO)," *Inf. Sci.*, vol. 373, pp. 337–350, Dec. 2016.

[38] D. Yu, J. Hong, J. Zhang, and Q. Niu, "Multi-objective individualized-instruction teaching-learning-based optimization algorithm," *Appl. Soft Comput.*, vol. 62, pp. 288–314, Jan. 2018.

[39] J. Aghaei, N. Amjady, and H. A. Shayanfar, "Multi-objective electricity market clearing considering dynamic security by lexicographic optimization and augmented epsilon constraint method," *Appl. Soft Comput.*, vol. 11, no. 4, pp. 3846–3858, Jun. 2011.

[40] R. V. Rao, V. J. Savsani, and D. P. Vakharia, "Teaching–learning-based optimization: An optimization method for continuous non-linear large scale problems," *Inf. Sci.*, vol. 183, no. 1, pp. 1–15, Jan. 2012.

[41] R. V. Rao, V. J. Savsani, and J. Balic, "Teaching–learning-based optimization algorithm for unconstrained and constrained real-parameter optimization problems," *Eng. Optim.*, vol. 44, no. 12, pp. 1447–1462, Mar. 2012.

[42] R. V. Rao, *Teaching Learning Based Optimization Algorithm: And Its Engineering Applications*. Cham, Switzerland: Springer, 2016.

[43] M. Črepinšek, S.-H. Liu, and L. Mernik, "A note on teaching–learning-based optimization algorithm," *Inf. Sci.*, vol. 212, pp. 79–93, Dec. 2012.

[44] J. K. Pickard, J. A. Carretero, and V. C. Bhavsar, "On the convergence and origin bias of the teaching-learning-based-optimization algorithm," *Appl. Soft Comput.*, vol. 46, pp. 115–127, Sep. 2016.

[45] C. A. C. Coello, G. B. Lamont, and D. A. Van Veldhuizen, *Evolutionary Algorithms for Solving Multi-Objective Problems*. Boston, MA, USA: Springer-Verlag, 2006. [Online]. Available: https://link.springer.com/book/10.1007%2F978-0-387-36797-2#about

[46] K. Deb, A. Pratap, S. Agarwal, and T. Meyarivan, "A fast and elitist multiobjective genetic algorithm: NSGA-II," *IEEE Trans. Evol. Comput.*, vol. 6, no. 2, pp. 182–197, Aug. 2002.

[47] E. Zitzler, K. Deb, and L. Thiele, "Comparison of multiobjective evolutionary algorithms: Empirical results," *J. Evol. Comput.*, vol. 8, no. 2, pp. 173–195, Jun. 2000.

[48] C. A. C. Coello, G. T. Pulido, and M. S. Lechuga, ''Handling multiple objectives with particle swarm optimization,'' *IEEE Trans. Evol. Comput.*, vol. 8, no. 3, pp. 256–279, Jun. 2004.
[49] S. Mirjalili, S. Saremi, S. M. Mirjalili, and L. D. S. Coelho, ''Multi-objective grey wolf optimizer: A novel algorithm for multi-criterion optimization,'' *Expert Syst. Appl.*, vol. 47, pp. 106–119, Apr. 2016.
[50] J. Fliege and A. I. F. Vaz, ''A method for constrained multiobjective optimization based on SQP techniques,'' *SIAM J. Optim.*, vol. 26, no. 4, pp. 2091–2119, Oct. 2016.
[51] A. I. F. Vaz. (Oct. 2015). *MOSQP Solver: Home Page*. Accessed: Jul. 14, 2018. [Online]. Available: http://www.norg.uminho.pt/aivaz/MOSQP/
[52] K. Deb, L. Thiele, M. Laumanns, and E. Zitzler, ''Scalable test problems for evolutionary multiobjective optimization,'' in *Evolutionary Multiobjective Optimization*. New York, NY, USA: Springer, 2005, pp. 105–145.
[53] H. Li and Q. Zhang, ''Multiobjective optimization problems with complicated Pareto sets, MOEA/D and NSGA-II,'' *IEEE Trans. Evol. Comput.*, vol. 13, no. 2, pp. 284–302, Apr. 2009.
[54] S. Garcia, D. Molina, M. Lozano, and F. Herrera, ''A study on the use of non-parametric tests for analyzing the evolutionary algorithms' behaviour: A case study on the CEC'2005 special session on real parameter optimization,'' *J. Heuristics*, vol. 15, pp. 617–644, Dec. 2009.

ELANGO NATARAJAN received the Ph.D. degree in mechanical engineering from Anna University, Chennai, India, in 2010. In 2013, he joined UTM, Skudai, Malaysia, as a Post-Doctoral Research Fellow. He has served for engineering colleges or universities for about 18+ years in various academic positions. Since 1999, he has been teaching mechanical engineering courses and he has gained extensive knowledge and experience in engineering design and stress analysis, CAE, vibration, statics, soft robotics, and polymer composites. He is a Chartered Engineer in mechanical with specialization in mechanical engineering design, CAE, and soft robotics. He is currently an Assistant Professor with the Faculty of Engineering, Technology and Built Environment, UCSI University, Kuala Lumpur, Malaysia. He is an active member of IET and the IEEE professional bodies.

VARADARAJU KAVIARASAN is currently pursuing the Ph.D. degree (part-time) in optimization of composite materials with Anna University, Chennai. Since 2007, he has been with the Sona College of Technology, India. He is teaching mechanical engineering course for undergraduate and postgraduate students.

WEI HONG LIM received the B.Eng. degree in mechatronic engineering and the Ph.D. degree in computational intelligence from Universiti Sains Malaysia, Malaysia, in 2011 and 2014, respectively.

From 2015 to 2017, he was a Post-Doctoral Researcher with the Department of Electrical Engineering, National Taipei University of Technology, Taipei. He is currently an Assistant Professor with the Faculty of Engineering, Technology and Built Environment, UCSI University, Kuala Lumpur, Malaysia. His research interests include demand side management and application of computational intelligence in engineering applications.

SEW SUN TIANG received the B.Eng. degree in electronic engineering (telecommunications) from Multimedia University, Malaysia, in 2008, and the Ph.D. degree in electrical and electronic engineering from Universiti Sains Malaysia, Malaysia, in 2014.

From 2015 to 2017, she was a Senior Lecturer with the School of Engineering, Asia Pacific University, Kuala Lumpur, Malaysia. She is currently an Assistant Professor with the Faculty of Engineering, Technology and Built Environment, UCSI University, Kuala Lumpur. Her research interests include medical applications of microwaves, and antenna design and optimization.

TENG HWANG TAN received the M.Sc. and Ph.D. degrees in electrical and electronic engineering from Queen's University Belfast, U.K., in 2008 and 2014, respectively.

He is currently an Assistant Professor with the Faculty of Engineering, Technology and Built Environment, UCSI University, Kuala Lumpur, Malaysia. He has more than eight years of teaching, industry, and research experiences. His research areas of interests are MEMS, instrumentation and measurement, wireless sensor network, and optimization of parameters.